



# Revisit of prevailing practice guidelines and investigation of topographical treatment techniques in CFD-Based air ventilation assessments

Karl An<sup>a,\*</sup>, Sze-Ming Wong<sup>a</sup>, Jimmy Chi-Hung Fung<sup>a,b</sup>, Edward Ng<sup>c</sup>

<sup>a</sup> Division of Environment and Sustainability, The Hong Kong University of Science and Technology, Hong Kong, China

<sup>b</sup> Department of Mathematics, The Hong Kong University of Science and Technology, Hong Kong, China

<sup>c</sup> Department of Architecture, Chinese University of Hong Kong, Hong Kong, China

## ARTICLE INFO

### Keywords:

Terrain modeling  
Air ventilation assessments  
Best practice guidelines  
CFD simulations

## ABSTRACT

Computational fluid dynamics (CFD) is a mature method in wind engineering studies, but many air ventilation assessment (AVA) reports prepared by consulting firms in Hong Kong still suffer from the use of inappropriate techniques and computational settings in the CFD modeling stage. The main reason behind this is the lack of informative guidelines relating to CFD model settings in the AVA Technical Circular issued by local authorities. Other aspects of AVA that require improvement include terrain modeling techniques and understanding the sensitivity of modeled topographical size to the wind environment.

This paper revisits and summarizes important aspects of current best-practice guidelines for robust CFD simulations. The study compares two conventional approaches to terrain treatment through a series of sensitivity tests. The first approach uses terrain features to cover the entire ground of the computational domain, whereas the second imitates wind tunnel experiments in which the domain includes an inclined buffer area. One drawback of the first approach was found to be the occurrence of numerical divergence when the terrain size is small; meanwhile, in the latter approach, the inclination angle of the buffer area must not exceed 30° to achieve robust results.

The final stage of the study validates the results of CFD simulations based on the two approaches with experimental data from a dense city. The approach that mimics wind tunnel experiments with a buffer zone was found to achieve better correlations, and smaller normalized mean square errors with respect to the experimental data and is thus considered superior.

## 1. Introduction

### 1.1. Background

In 2003, to prevent the construction of poorly designed developments that would negatively affect the air ventilation performance of local neighborhoods, the Planning Department of the Hong Kong SAR Government adopted an initiative that requires both governmental and non-governmental developers in Hong Kong to undertake air ventilation assessments (AVAs) [1–3] for their proposed development projects. Ng [4,5] assisted in the development of the AVA framework and guidelines, and an AVA Technical Circular (AVA TC hereafter) was published by the Housing, Planning and Lands Bureau [6].

In the years since the launch of the AVA system, developers in Hong Kong have shown increasing awareness of air ventilation as a critical

environmental factor in their projects. This has led to great improvements in building morphology designs.

In addition, practices related to AVA have been increasingly promoted in other Asian and European countries. Cities differ with respect to the critical issues and concerns around air ventilation, depending on their geographic location and urban density. High-density cities, mostly in Asia, are particularly reliant on sufficiently strong winds for ventilation. In contrast, in European cities with a smaller urban density, the focus is generally placed on the possibility of wind gusts and amplification problems. However, regardless of the differences among wind ventilation studies in terms of their research focuses or experimental approaches (e.g., numerical modeling, wind tunnel experiments), they share the need to follow prevailing practice guidelines to ensure robust outcomes for these assessments. Moreover, depending on the assessment location, the treatment of the local topography is frequently a challenge.

\* Corresponding author. The Hong Kong University of Science and Technology, Division of Environment and Sustainability, Clear Water Bay, Hong Kong, China.  
E-mail address: [karl.an@connect.ust.hk](mailto:karl.an@connect.ust.hk) (K. An).

Therefore, it is worthwhile to revisit the prevailing guidelines and summarize the important points to consider during numerical modeling, as well as to carry out a more in-depth study on terrain treatment techniques.

### 1.2. Literature review

Computational fluid dynamics (CFD) is a powerful and widely popular tool among environmental scientists, engineers, architects, developers, and planners to carry out parametric studies to explore optimum building design strategies while providing scientific support to the proposed city designs. The results of CFD simulations help planners to prevent disastrous environmental effects that threaten human health and life as a result of the construction of their proposed developments.

In conjunction with wind tunnel experiments and field measurements [7–12], CFD has proven to be among the most successful tools for simulating and for gaining an understanding of the continuously changing mechanisms within an urban boundary layer. This approach has also been applied to understand the external flow environment of cities to aid design processes [13–26]. Developers now rely on CFD to explore optimum designs to maximize the saleable areas of their properties while maintaining good ventilation performance.

Accurate CFD simulations with validated performance are powerful tools to model wind flow and pollutant dispersion problems in both idealized and real urban areas [20,27–31]. CFD can provide complete data for the flow and concentration field within the computational domain and can be performed at both reduced and full scales. In addition, CFD models enable efficient parametric and sensitivity analysis [32–43] and, most importantly, can provide intuitive visualization to aid the understanding of complex ongoing physical processes within an urban canopy.

In the past decade, extensive AVA studies have been conducted using CFD with reference to the guidelines stated in the AVA TC. However, although the content of this technical circular is grounded on existing research, it was published more than a decade ago and has not been technically refined or revised in terms of CFD modeling methodologies since then. A particular clause in the AVA TC comments on the use of CFD in AVA studies: “Computational Fluid Dynamics (CFD) may be used with caution; it is more likely admissible for the Initial Studies. There is no internationally recognized guideline or standard for using CFD in outdoor urban scale studies. The onus is on the assessor to demonstrate that the tool used is ‘fit for the purpose’.”

The best practice guidelines have undergone rapid developments in the past ten years, and many successful studies have examined wind-engineering problems using CFD. This implies that CFD is now a mature method supported by up-to-date international guidelines for performing air ventilation studies [44–47]. The aforementioned clause in the AVA TC is therefore considered inapplicable.

Apart from that, a research team led by Ng et al. carried out a feasibility study to further refine the Air Ventilation Assessment System for Hong Kong and published a report titled “Urban Climatic Map and Standards for Wind Environment” in 2012 [3]. In their report, refinements for the AVA TC were recommended. These refinements suggested the inclusion of wind performance criteria for AVA studies in Hong Kong, provision of a set of standard site wind availability data, and informative documentation of the model settings for Air Ventilation Assessments via CFD modeling. Regrettably, most of the recommendations have not yet been incorporated into the AVA TC by local authorities.

### 1.3. Objectives

Owing to certain ambiguity aspects in the AVA TC, in addition to incomplete knowledge of the CFD literature and best practice guidelines in the field, many consultancy CFD simulations and reports still display a major lack of a basic understanding of fluid mechanics, numerical

techniques, and appropriate scientific assumptions [48]. Moreover, there appears to be a growing tendency for the environmental consultancy industry to extend the CFD approach to other environmental assessments, which include but are not limited to indoor/outdoor pollutant dispersion simulations and thermal comfort simulations [30, 49]. The time seems appropriate to provide a retrospective review and supplement the missing details in the AVA TC by reference to mature international guidelines and recommendations to furnish a refined and complete circular for the consultancy industry to follow.

Hong Kong’s terrain is hilly and mountainous with steep slopes, which makes the inclusion of terrains in CFD modeling unavoidable for most industrial projects. Terrain modeling is a key challenge in industrial projects that use CFD. Various approaches are used to incorporate terrain within the computational domain, and debates continue within the industrial community regarding the merits of these approaches.

The aim of this paper is to revisit the main aspects of the best practice guidelines and to summarize the essential points regarding each aspect to allow supplementation in the CFD modeling context of the AVA TC. The major focus is placed on discussion and exploration of the appropriate ways to model and incorporate terrains within the computational domain for a microscale CFD study. The study is carried out systematically, and the simulation results from the approaches adopted are validated by wind tunnel experimental data.

To promote the evolution of CFD into a state-of-the-art tool in environmental assessments, the last section discusses the methods’ limitations and proposes potential improvements in the application of CFD in wind flow studies for environmental assessors/consultants to contemplate.

### 1.4. Structure of the paper

Following the introduction section, the Best Practice Guidelines for AVA via the CFD approach are reviewed. Fundamental but important aspects which include the choice of turbulence models, the scale of projects, simplification of modeled obstacles in the simulations, the extent of the computational domain, establishment of the initial and boundary conditions, the amount and size of computational grids, and numerical schemes and convergence criteria, were summarized in section 2.

After the revisit of BPGs, the focus was put on the comparison of two terrain modelling approaches in CFD simulations through a series of sensitivity tests supported by wind tunnel validation. The detailed description of the two terrain treatment approaches and geometrical setups of the investigated cases were presented in section 3. Following section 3, sections 4 and 5 documented the setup of the wind tunnel experiment and the CFD settings for the simulated cases, respectively. Moreover, specific grid sensitivity tests have been conducted, and the results were also given in section 5. Discussions and comparative analysis of the CFD sensitivity testing results for the series of cases were carried out in section 6, together with the presentation of wind tunnel validation results. The study was then concluded by several major insights that were given in section 7.

## 2. Review and revisit of best practice guidelines for AVA via CFD

Various researchers [47,50,51] have provided Best Practice Guidelines (BPGs hereafter) for CFD in pedestrian wind environment assessments. These guidelines are based on consideration of basic CFD concepts, literature reviews, sensitivity studies on various computational parameters, and cross-comparison/validation results with wind tunnel or field measurement data. The development of BPGs aims to cover as many aspects as possible in an attempt to provide clear directions and complete information on the CFD approach in wind engineering simulations.

The existing BPGs (most importantly the COST 732 guidelines [51] and AIJ guidelines [47,77]) outline instructions on several aspects

encountered by CFD modelers when applying this tool in the simulation of urban wind environments. These include the choice of turbulence models, simplification of modeled obstacles in the simulations, the extent of the computational domain, establishment of the initial and boundary conditions, the amount and size of computational grids, numerical schemes and convergence criteria.

### 2.1. Geometrical representations of obstacles

Simplification is essential and ubiquitous in the pre-processing stage of CFD simulations. Too many detailed features will increase the difficulty in generating a good quality mesh and may prevent the CFD solver from reaching a numerically stable solution. As explored by Franke et al. [51], although it is important for the central area of interest to be reproduced with detailed features, increased detail requires more cells to resolve. Therefore, the feasible level of detail in the geometric representation of obstacles is limited by the available computational resources.

Although conceptually simple and dependent on the judgment and experience of CFD modelers, it is important that features, which generate important turbulence phenomena and affect the wind flow pattern, would not be omitted during simplification. Small structures such as lampposts and pedestrian footbridges can generally be excluded. Fig. 1 illustrates an example of geometry simplification.

### 2.2. Terrain modeling

Despite the BPGs' attempt to cover as many aspects as possible for the application of CFD in simulations of urban wind environments, informative guidelines on the treatment of terrains and methods of their incorporation into the computational domain are lacking. The current approach to terrain treatment is arbitrary relative to other aspects of CFD modeling. Two main approaches (see Fig. 2) are used to model the terrain features in current practice: (1) with the modeled terrain covering the entire ground of the computational domain, or (2) with the model terrain set upon a turntable, bounded by buffer areas, and placed at the center of the computational domain to mimic the approach used in wind tunnel experiments. One of the focuses of this paper is to compare in detail the outcomes of these two modeling approaches, as presented systematically in Sections 3 to 5.

### 2.3. Choice of turbulence models

The choice of the turbulence model is critical in CFD simulations. Ferziger [52] noted that the chosen method and turbulence model should depend on the required prediction accuracy, computation time, and the investigated problem itself. Reynolds-averaged Navier-Stokes (RANS) methods can provide "sufficiently accurate" results and remain the dominant choice in industrial applications [53,54]. Gosman [55], Yoshie et al. [56], and Baker [57] have confirmed that CFD RANS is appropriate for pedestrian wind comfort problems.

The COST 732 BPG and AIJ guidelines provide no specifications for

which turbulence model should be used in CFD simulations of wind environments in urban and industrial areas. That said, COST 732 indicates that the turbulence model should be validated against a simpler geometry that retains the critical features to evaluate the model's performance. Some advanced unsteady models, such as large-eddy simulations (LES) or detached eddy simulations (DES) that can solve a larger portion of the turbulence spectrum than steady-state eddy-viscosity models, require substantially more computational time and resources than RANS. Most importantly, these advanced models still lack mature technical guidelines and practical experience among the industrial community. In contrast, simulation of wind fields by CFD RANS has reached a mature state, with well-developed technical guidelines [44–47] and extensive experience through a long history of the practice.

Owing to the need for a balance between accuracy and computational cost, most studies of outdoor advection-dominated wind ventilation problems adopt RANS as the turbulence model to provide satisfactory validation results [58–75]. In environmental simulations, to shorten the design and marketing cycle, the RANS turbulence model will continue to play an important role, especially in industrial and environmental computations [48,76].

However, the results obtained by Mochida et al. [77] and Franke et al. [44] imply that prototype versions of eddy-viscosity models (i.e., the standard  $k - \epsilon$  model) should be avoided in simulations of the wind environment of urban areas, whereas modified eddy-viscosity models [78,79] are preferable.

### 2.4. Size of computational domain

The extent of the computational domain generally depends on the simulation of the geometries. Various researchers [80–82] recommend a lateral and vertical extension of  $5H_{tall}$  from the built area, where  $H_{tall}$  is the tallest building height. The intent of incorporating the distances between buildings and their boundaries into the computational domain is to avoid artificial wind acceleration at the edges of buildings. Further to the lateral and vertical extension, the existing BPGs also provide suggestions regarding the size of the domain in the streamwise direction. A distance of  $5H_{tall}$  is recommended between the inflow boundary and the built areas to allow the flow to develop. However, if detailed information on the inflow wind profile is lacking, the inflow boundary must be extended further away. To allow the flow to fully develop at the wake region, the outflow boundary of the computational domain downstream of the built area should not be placed less than  $15H_{tall}$  from the buildings, as suggested by Cowan et al. [81], Scaperdas and Gilham [82], and Bartzis et al. [83].

### 2.5. The setting of boundary conditions

Both the AIJ guidelines and COST 732 BPGs indicate that a zero normal velocity and zero normal gradients of the tangential velocity should be implemented for the upper and lateral boundaries of the computational domain. The downstream boundary condition is recommended to be zero normal gradients for all variables, and the boundary conditions of all solid surfaces are suggested to be set as no-slip walls.

### 2.6. The setting of inflow conditions

Inflow profiles usually contain information on the mean velocity and turbulence quantities, must be imposed at the inlet boundaries to drive the CFD model. The requirement in the robustness of the inflow turbulent profile (in terms of magnitude) is less strict than the need for an accurate inflow wind profile, as reported by An et al. [84]. These inflow profiles are commonly obtained from wind tunnel experiments and simulation outputs from meteorological models (e.g., WRF or RAMS).

Although it is suggested by the COST 732 BPGs that wind tunnel data are the preferable data source for the approximation of inflow profiles, topographical studies using wind tunnel are not capable of providing

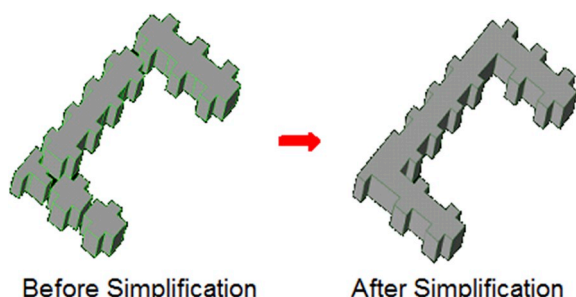


Fig. 1. Illustration of geometry simplification.

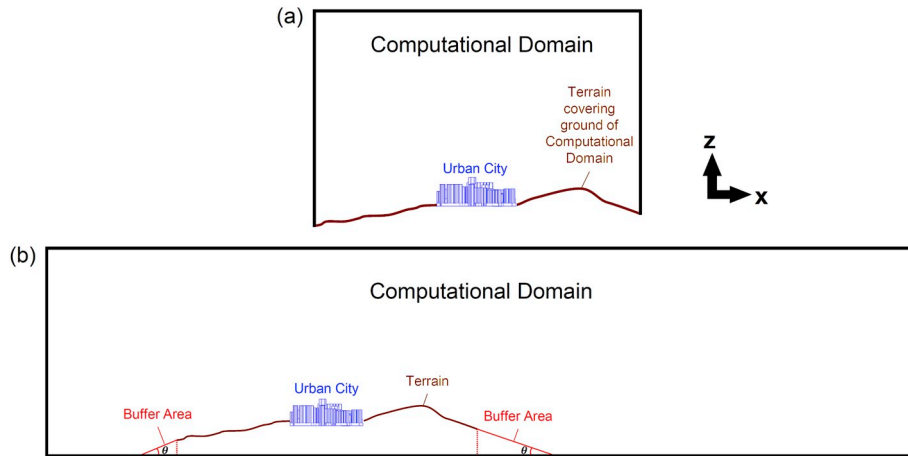


Fig. 2. Illustration of terrain treatment techniques (a) Approach A (b) Approach B.

representative site wind availability data for coastal areas with land-sea breezes. Therefore, wind tunnel can be adopted in conjunction with meteorological models that can overcome this particular weakness and produce a set of fine-grid site wind availability data that take into account the surrounding terrain features and atmospheric conditions.

### 2.7. Computational grid

The near-wall flow is typically composed of three sub-layers. They are a laminar sub-layer in which the mean velocity is linearly related to the non-dimensional wall distance  $y_+$ , a fully turbulent sub-layer in which the mean velocity and  $y_+$  shows a logarithmic relationship, and a transitional sub-layer which connects the two sub-layers mentioned above. There are mainly two approaches to resolve the flows in the near-wall region. One way is to adopt wall functions that use semi-empirical formulas to bridge the viscosity-affected region between the wall and the fully-turbulent region. The wall function approach does not need to resolve the boundary layer and would result in a reduction of mesh amount in comparison to the second way, which resolves the viscosity-affected region with very fine meshes down to the wall.

The most suitable inflation mesh for the geometry is strongly tied to the choice of the turbulence model and to the characteristics of the flow field that one is interested in capturing. The AIJ guidelines indicate that the minimum grid resolution should not be coarser than 1/10 of the building scale, and sufficiently fine near-wall cells are required to accurately predict flow behaviors near the wall region, preferably maintaining a sufficiently small non-dimensional cell wall distance  $y_+$  for the first layer of cells next to the wall surfaces.

For steady RANS  $k - \epsilon$  family models, which adopt the standard wall function approaches, the value of the non-dimensional wall distance  $y_+$  should be maintained in the range of 30–500. On the contrary, for unsteady LES models or  $k - \omega$  family models, which solve the flow down to the viscous sublayer instead of adopting wall function approaches, a smaller value of  $y_+$  less than unity is preferable.

In view of the need to balance the prediction accuracy, the numerical stability, and the computational costs, slight relaxation of the restriction in  $y_+$  value should be allowed. With numerical convergence as a priority, one should always attempt to keep  $y_+$  as small as possible. As a rule of thumb, it is considered the good practice to include 4 to 10 inflation mesh layers within the boundary layer to robustly resolve flow structures within the layer and accurately predict any separation or reattachment points.

### 2.8. Numerical schemes and convergence criteria

The first-order upwind scheme is considered incapable of producing

accurate enough simulation results. Less diffusive higher-order numerical schemes are favorable. Meanwhile, given the need to maintain numerical stability, the relaxation factors can be adjusted. However, one drawback in reduction of relaxation factors is a slower rate of convergence and longer computational time.

Existing guidelines suggest that a sufficient convergence criterion for CFD simulations of wind engineering problems is that the scaled residuals for all variables drop below  $1 \times 10^{-4}$  [85]. To ensure that the simulated solutions have reached a steady state, convergence tests should be carried out. These are performed by monitoring the variables of interest until they exhibit non-observable changes, taken as an indication that they have reached a stable and converged solution.

### 2.9. Scale of projects

There has been a tendency of increasing the scale of the industrial projects that adopt CFD to carry out AVAs (the largest project involved a site area >300 ha). In principle, with enough fine grid cells (on the scale of hundreds of millions), enough time, and sufficient computer resources (depending on the type of turbulence model adopted), CFD can provide robust wind flow patterns.

In view of the nature of CFD models (i.e., microscale models applied to simulate a variety of details), regardless of the available computational resources and computational time in the industrial field, project sites on very large scales are not considered feasible unless such simulations aim only to offer broad patterns of wind flow.

Therefore, for CFD simulations of development areas on such scales, a more appropriate approach is to break down the total area into sites of smaller scales (i.e., on the magnitude of several tens of hectares). Separate CFD simulations should then be carried out on each of these small-scale sites with mesh cell counts on the magnitude of several million for steady RANS models or even more for higher classes of unsteady models.

## 3. Terrain modeling and buffer area simplification

### 3.1. Different approaches in treatment of terrains

The terrain inevitably influences the wind flows that reach a city. The inclusion of topographical features in industrial AVA projects is an essential yet challenging task. Debates have been ongoing between environmental assessors and consultants on the extent to which terrain features should be modeled, and the modeling approach itself for the inclusion of topographical features within the computational domain.

One relatively direct approach is to include terrain features that cover the entire ground of the computational domain (denoted

Approach A hereafter, see Fig. 2a) [86–88], and another (Approach B hereafter, see Fig. 2b) [26,89,90] is to imitate the practice in wind tunnel experiments, in which the modeled terrain is placed upon a turntable within the computational domain. For analysis of airflow over steep topography in the latter approach, a buffer area is established. The terrain in the buffer area is relatively flat but with a slight elevation and connects smoothly to the terrain in the computational domain.

Despite the incorporation of the flat and gently rising buffer area in Approach B, which allows a smooth transition of wind and turbulence profiles before reaching the true terrain to ensure better convergence, the creation of buffer zones is relatively arbitrary. There are no guidelines on the generation of buffer zones, and this step is highly dependent on the judgment of the CFD modelers. It has been argued that the buffer zone can result in distortion of the vertical wind profile before it reaches the real terrain and affects the simulated wind flow patterns and magnitude if the buffer zones are modeled inappropriately or the extent of the modeled terrain is in close proximity to the dense urban area of interest. The above concerns regarding the buffer zones are investigated in detail in this paper. Furthermore, this paper investigates the sensitivity to the terrain size and compares the advantages and disadvantages of Approaches A and B.

### 3.2. Simulated cases

Four series with 21 cases have been simulated. This study was carried out in a progressive manner, starting from a series of five ideal cases (A-1, A-2, A-3, A-4, and A-5), focusing on the treatment of buffer areas in Approach B. These ideal cases were designed to model a conceptual dense urban area situated on flat land with different inclination angles of the buffer area, aiming to determine the optimal angle. Following Cases A, another four cases (B-1, B-2, B-3, and B-4) were constructed to reinforce the findings of Cases A, by replacing the flat land with hilly terrain (see Fig. 3). Through the insights gained from the simulation results of Cases A and B, an appropriate way to create a buffer area that does not greatly alter the robustness of the results can be established.

The study further progressed by investigating the influence of terrain size on the CFD simulation results. Approach A and Approach B were both applied to another eight cases (C-1A to C-4A and C-1B to C-4B) with different terrain extents  $xR$  calculated from the edges of the simulated urban area, where  $R = 500m$  and  $x = 1, 2, 3, 4$  corresponding to Cases C-1 to C-4 respectively. Therefore, Cases C-1A, C-1B have the smallest terrain size with an extension of  $1R = 500m$  from the simulated urban area edge while Cases C-4A, C-4B have the largest extension distance of  $4R = 2000m$ . This series of cases (see Fig. 4) explored the sensitivity of the modeling results to the size of the terrains and whether variation in modeling techniques affected the consistency of the outcomes.

The final stage of the study validated the CFD results obtained by Approaches A and B, under different terrain sizes, against wind tunnel experiment data on a real urban environment via Cases D-1 to D-4 (see Fig. 5). The results are intended to help determination of the most favorable approach to terrain incorporation in AVA studies that adopt CFD as a modeling tool, at the same time, reinforce and provide supplementary information on terrain modeling in the current AVA TC. The major design concepts and parameters of the investigated cases are

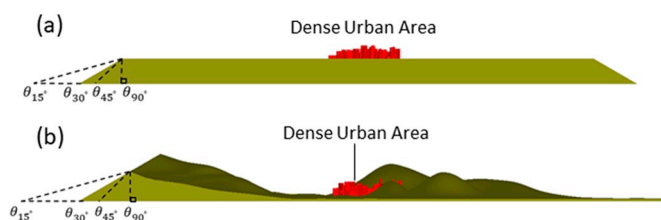


Fig. 3. Inclination angles of buffer area for (a) Cases A (b) Cases B.

summarized in Table 1.

### 3.3. Air ventilation indicator

The wind velocity ratio (VR) [91], a dimensionless number, is the indicator most commonly used to assess pedestrian wind comfort in AVA studies. This indicator is adopted here as the wind performance indicator and is defined as:

$$VR = \frac{V_P}{V_\infty} \quad (1)$$

where  $V_\infty$  is the wind velocity at the top of the wind boundary layer and is not affected by the ground roughness or local site features, whereas  $V_P$  is the wind velocity at the  $2m$  pedestrian level. VR indicates how much of the wind availability is experienced by pedestrians on the ground and allows a relatively simple indication of the study site's wind environment. The higher the value of VR, the better the air ventilation performance.

### 3.4. Performance metrics

In addition to the correlation value between measured and simulated results, two other validation metrics were used to quantify the agreement between the simulation and experimental results [92]: the fraction of the prediction within a factor of 2 of the observations (FAC2) and normalized mean square error (NMSE). These metrics can be expressed as follows:

$$FAC2 = \frac{1}{N} \sum_{i=1}^N n_i \text{ with } n_i = \begin{cases} 1 & \text{for } \left(0.5 \leq \frac{P_i}{M_i} \leq 2\right) \cup (M_i \leq W \cap P_i \leq W) \\ 0 & \text{else} \end{cases} \quad (2a)$$

$$NMSE = \frac{\overline{(P_i - M_i)^2}}{\overline{P} \times \overline{M}} \quad (2b)$$

where  $M_i$  and  $P_i$  are the measured and predicted values of a given variable for sample  $i$ , respectively; and  $N$  is the number of data points. The overbars denote the mean of the dataset. The allowed absolute difference  $W$  was set to 0.05 for FAC2. An ideal model would produce metric values of 1.0 for FAC2 and 0 for NMSE.

## 4. Wind tunnel experiment setup for validation

The details of the wind tunnel settings for validation were documented in the published experimental report, and only the main features are presented here. The experiment was performed using the CLP Power Wind/Wave Tunnel Facility (WWTF) at the Hong Kong University of Science and Technology. The wind tunnel study was undertaken in accordance with the requirements stipulated in the Australasian Wind Engineering Society Quality Assurance Manual (AWES-QAM-1-2001) [93] and the American Society of Civil Engineers Manual and Report on Engineering Practice No. 67 for Wind Tunnel Studies of Building and Structures [94].

The wind tunnel facility comprises two long fetch boundary layer wind tunnel test sections, as shown in Fig. 6a. The high-speed test section, which is  $28m$  in length, has a  $3m$  wide  $\times$   $2m$  high working section with a maximum freestream wind speed of approximately  $30m/s$ . The  $40m$  long low-speed test section has a  $5m$  wide  $\times$   $4m$  high working section and a maximum freestream wind speed of approximately  $10m/s$ . Various terrain simulations can be modeled in either test section at length scales ranging from approximately 1:5000 to 1:50.

A 1:400 scale model that included all known existing and approved developments and topographical features within a radius of

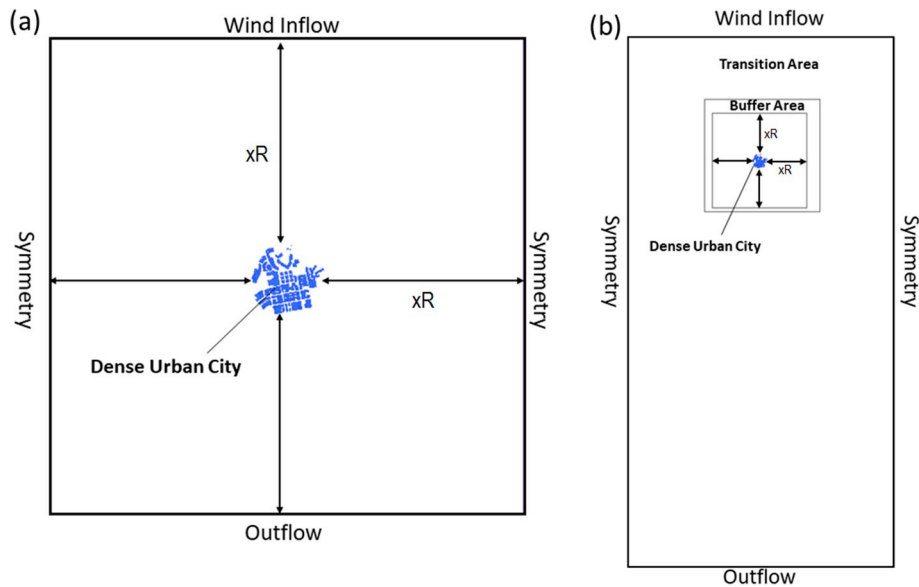


Fig. 4. Illustration of modeled computational domains for Cases C via (a) Approach A, (b) Approach B.

approximately 600m from the center of the Project Area (where the blue colored buildings are located in Fig. 6b) was fabricated to represent the current state of the urban areas.

Sensors were installed at the height of approximately 2m above ground level at prototype scale (i.e., 5mm at the model scale) and wind speeds at the test points (see Fig. 6d) were measured using a multi-channel thermal anemometer whose signals were sampled using a dedicated computer for a period of approximately 1 hr at the prototype scale.

To achieve a fair comparison between the CFD simulation results and wind tunnel data, a 1:400 CFD model with topographies and building morphologies as close as possible to the wind tunnel experiment was constructed (see Fig. 6c). In addition, the Reynolds number of the CFD model and the wind tunnel experiment was kept consistent.

Although pedestrian level wind speed measurements were taken at 22.5° increments across the full 360° azimuth (i.e., 16 wind directions) in the wind tunnel experiment, the northerly wind coming from the sea was considered to be more representative when compared to the southerly wind which would be sheltered by the terrains and anticipated to have a comparatively lower wind magnitude. Apart from the above reason, the northerly wind is also one of the major prevailing wind directions towards the Project Area in this wind tunnel experimental study, therefore without loss of generality, the measurement data of the northerly wind were taken for model validation.

## 5. CFD simulation settings

### 5.1. Computational domain

The computational domains adopted in this study were all rectangular. For the Cases A to D that adopted Approach B, size of the computational domains comply with the CFD guidelines [45,47]. For Cases C-1A to C-4A, which adopted Approach A, the dimensions from the computational domain boundaries were at least  $1R = 500m$  (Case C-1A) in all horizontal directions from the simulated city edge, increasing incrementally to  $4R$  in Case C-4A. The vertical extent of the computational domain more than  $1.5R$  for all Cases C-1A to C-4A.

### 5.2. Inflow profiles

For Cases A to C, the inflow wind profile was a typical atmospheric power law wind profile in the form of  $U(z) = U_H(z/H)^n$ , whereas the

turbulent kinetic energy profiles were in typical functional forms of  $k(z) = \eta_1 z^{\eta_2} \exp(-\eta_3 z)$ . The turbulence dissipation rate,  $\epsilon$  was estimated using the equation  $\epsilon = C_\mu^{0.75} k^{1.5} / \kappa z$ , where  $C_\mu = 0.09$ ,  $k$  is the turbulent kinetic energy, and  $\kappa = 0.4$  is the von Karman constant. The constants for the profiles were set with  $U_H = 8.2m/s$ ,  $H = 300m$  and wind index  $n = 0.18$  with  $\eta_1 = 1.61$ ,  $\eta_2 = 0.14$  and  $\eta_3 = 0.0018$ .

The CFD simulations for model validation (Cases D) adopted the fitted profiles of inflow wind and turbulent kinetic energy (see Fig. 7) of the northerly wind based on experimental data from the “Final Report for an Instructed Project at Ex-North Point Estate Site – WWTF Investigation Report WWTF015-2008” [95]. The inflow profiles were fitted to the wind tunnel data with standard functional forms of power-law wind profile and turbulence profiles by minimizing the mean squared error. The set of profile constants with values  $U_H = 8.2 m/s$ ,  $H = 0.75m$ , and the wind index  $n = 0.18$ , was found to generate the best fit of the experimental inflow wind profile, while the function  $k(z) = \gamma_{v1} z^{\gamma_{v2}} \exp(-\gamma_{v3} z)$ , with  $\gamma_{v1} = 3.69$ ,  $\gamma_{v2} = 0.14$  and  $\gamma_{v3} = 0.72$ , minimized the mean squared error when fitting the turbulent kinetic energy data from the wind tunnel database.

The commercial CFD code ANSYS FLUENT 14.5 (Fluent Inc., 2012) was used, which applies the finite-volume method to solve the three-dimensional equations of incompressible steady-state continuity and momentum. The realizable  $k - \epsilon$  model, a commonly used turbulence model in AVAs, was adopted for turbulence modeling with the standard wall function.

### 5.3. Boundary conditions, numerical schemes, convergence criteria, and mesh fineness

The boundary conditions, numerical schemes, and convergence criteria for Cases A to D were consistent with the description in Section 2, and were summarized in Table 2 for ease of reference.

On average, 10 million unstructured mesh cells were generated for Cases A and B. For Cases C, approximately 10 million unstructured mesh cells were generated with Approach A, whereas 12 million unstructured mesh cells were used with Approach B. The computational domain size and the approximate grid numbers for the cases in the validation study (Cases D) are tabulated in Table 3. For all the simulated cases, refined mesh grids were created near the street canyons and block obstacles with a minimum size of 2m and a maximum size of 4m, whereas coarser grids set with a maximum size of approximately 100m were adopted at regimes further from the buildings and topographical geometries. The

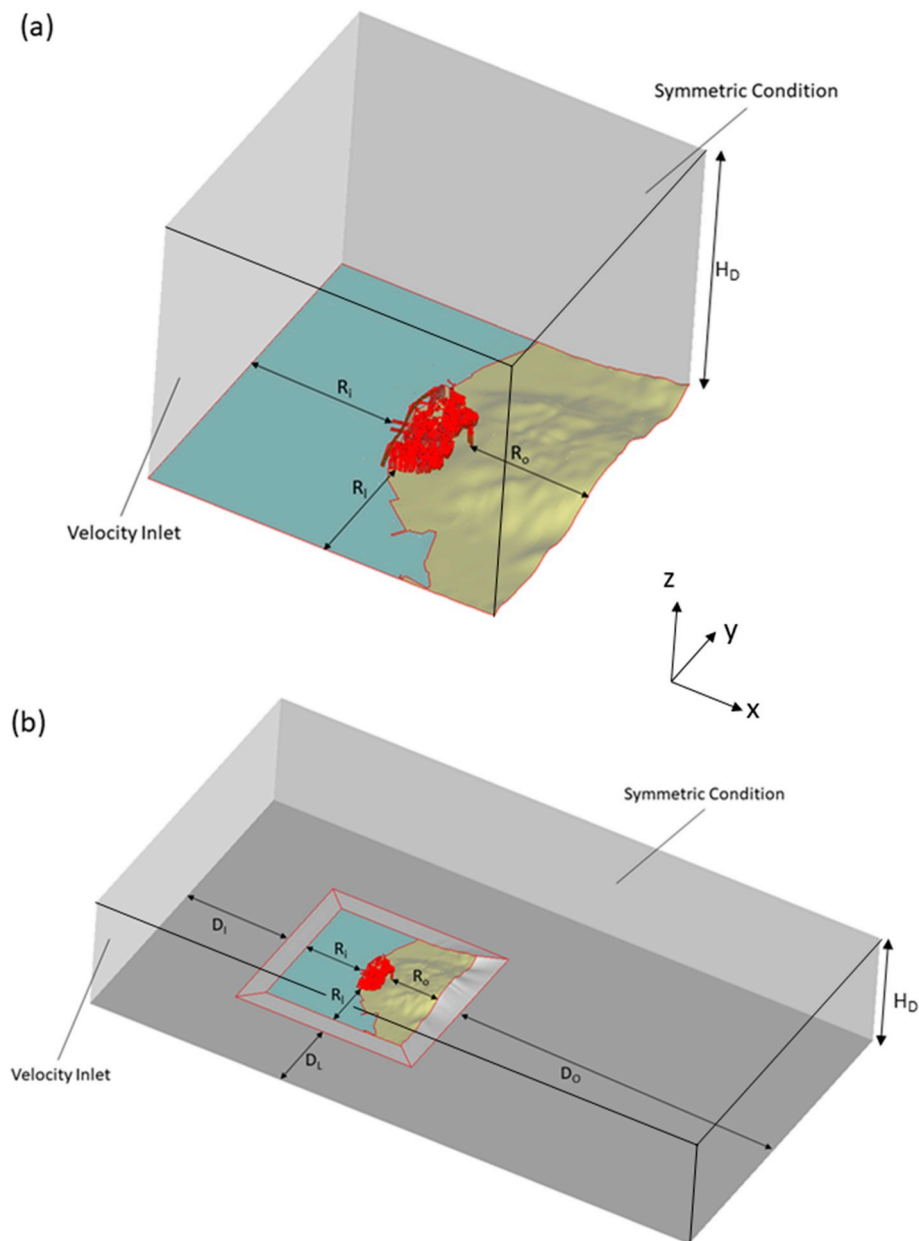


Fig. 5. Illustration of the computational domain for Cases D modeled via (a) Approach A, (b) Approach B.

vertical and horizontal grid expansion ratios also satisfied the criterion of being less than 1.2.

Furthermore, for all simulated cases in Cases A to C, unstructured grids with prismatic layers with a minimum size of  $0.025m$  were introduced around all wall faces ensuring average values of  $y_+$  in the optimal range of  $30 < y_+ < 300$ . For validation Cases D, four layers of boundary mesh covering all surfaces including building walls, with the first layer of mesh at an approximate distance of  $3 \times 10^{-4} m$  with an average value of  $y_+ < 5$  at model scale, were generated to capture the shearing boundary layer flow.

#### 5.4. Grid sensitivity

Three types of the grid were implemented to carry out grid sensitivity tests on the investigated Cases A to D. Because the results/conclusions from the grid sensitivity tests were similar for all cases, in the interest of brevity, only the results for Case B-2/Case C-3B and Case D-3 are presented here.

A basic grid with approximately 12.1 million cells and 8.4 million cells was generated for Case B-2/Case C-3B and Case D-3, respectively. The fine grid and coarse grid for the cases deviate from the basic grid by approximately  $\pm 20\%$  (see Fig. 8).

Fig. 9 compares the simulation results under the three types of grid in terms of the wind velocity ratios. There are no observable differences with an average absolute percentage error of approximately 5%, between the results from the basic and fine grids, the basic grid was considered sufficiently well resolved and was adopted for the simulated cases.

#### 6. Performance comparison

The building morphologies were the same for all three series of simulated cases. Test points were placed at 49 representative locations (divided into five groups) within the modeled conceptual urban area for Cases A, B, and C, as illustrated in Fig. 10.

Pedestrian level wind data at  $2m$  above the terrain were extracted at

**Table 1**  
Major design parameters of the investigated cases.

Test cases	Approach	Maximum angle of inclination for buffer area	Topographical features
Case A-1	B	15°	Flat terrain, 3R from the urban city edge
Case A-2		30°	
Case A-3		45°	
Case A-4		60°	
Case A-5		90°	
Case B-1	A	15°	Hilly terrain, 3R from the urban city edge
Case B-2		30°	
Case B-3		45°	
Case B-4		90°	
Case C-1A		–	
Case C-2A	B	30°	Hilly terrain, 1R from city edge to domain boundary
Case C-3A			Hilly terrain, 2R from city edge to domain boundary
Case C-4A			Hilly terrain, 3R from city edge to domain boundary
Case C-1B			Hilly terrain, 4R from city edge to domain boundary
Case C-2B			Hilly terrain, 1R from city edge to buffer zone
Case C-3B			Hilly terrain, 2R from city edge to buffer zone
Case C-4B			Hilly terrain, 3R from city edge to buffer zone
Case D-1			A
Case D-2	B	30°	Terrain extent at least 4R towards computational domain boundaries
Case D-3			Terrain extent mimics wind tunnel Experiment
Case D-4			Terrain extent at least 4R towards buffer zone boundaries

the test point locations, and the averaged wind velocity ratio ( $VR$ ) defined in Equation (3a) was used as a wind performance indicator. Apart from  $VR$ , the average vertical turbulent kinetic energies (from terrain level to a height of 500m) defined in Equation (3b) were also calculated and used as a comparison indicator.

$$VR_{average} = \frac{1}{n} \sum_{i=1}^n VR_i \quad (3a)$$

$$TKE_{average} = \frac{1}{n} \sum_{i=1}^n TKE_i \quad (3b)$$

where  $n = 49$ ,  $VR_i$  is the pedestrian wind velocity ratio at test point  $i$  and  $TKE_i$  is the vertical mean  $TKE$  from terrain level to a height of 500m at test point  $i$ .

### 6.1. Sensitivity to buffer zone inclination (Cases A and B)

Cases A and B adopted Approach B and involved an inclined buffer area in the CFD model. The ideal buffer area should be relatively flat and modeled with a small inclination angle that connects smoothly to the terrain. To achieve this, the inflow and outflow faces of the computational domain must be extended very far.

The smallest inclination for the buffer area of both Cases A and B was 15°. This angle is considered small enough to create a relatively flat buffer area with a gradual gradient that connects smoothly to the terrain that contains the modeled city. Any inclination of the buffer area less than 15° was assumed to produce average values of wind velocity ratio and turbulent kinetic energy that differ non-observably from the buffer-free case within the modeled dense urban area.

Fig. 11 plots the vertical wind velocity ratio and  $TKE$  profiles against normalized height ( $H = 50m$ ) for Cases A with flat terrain, averaged according to the five groups of test points (see Fig. 11). Similar profiles were obtained for Cases B with hilly terrain and were not presented here for the sake of brevity. It can be observed that the case with the  $\theta = 30^\circ$  buffer area inclination (Case A-2, red dashed line) deviates the least from the case with  $\theta = 15^\circ$  inclination (Case A-1, solid blue line) in all

groups for both the averaged wind and  $TKE$  profiles. When the inclination of the buffer area is increased to  $\theta = 45^\circ$  (Case A-3, black line with circles), the trends in wind and  $TKE$  profiles are qualitatively similar to Cases A-1/A-2, but with an observable deviation in profile magnitude. The deviation in magnitude is more obvious at the windward groups of test points (Groups 4 to 5) than the leeward groups (Groups 1 to 3).

After the inclination is further increased to  $\theta = 60^\circ$  and  $\theta = 90^\circ$  in Case A-4 and Case A-5 respectively, the averaged  $TKE$  profiles begin to deviate from the other cases in terms of both shape and quantitative magnitudes. This can be clearly seen from the averaged  $TKE$  profiles for the Groups 4 and 5 test points. For the averaged wind profiles, although the shape is maintained, the absolute values are under-predicted for Cases A-4 and A-5 relative to Case A-1.

Fig. 12 shows the pedestrian wind  $VR$  at the 49 test points for both Cases A and B. In terms of pedestrian wind environment, and the trend lines indicate that the change in the buffer area's inclination does not result in changes in the wind pattern at pedestrian level but does alter the predicted magnitude of the wind. For Cases A with flat terrain, an inclination of  $\theta = 45^\circ$  in the buffer zone can still produce a wind  $VR$  close to the case with an inclination of  $\theta = 15^\circ$ . However, for Cases B with hilly terrain, a difference of more than 25% in wind magnitude is observed between the 15° case and all cases with 45° inclination or beyond.

The data presented in Fig. 13 and Table 4 illustrate the results more clearly. For Cases A with flat terrain, a 30° inclination in the buffer area only results in a deviation of approximately 4.8% in terms of average wind  $VR$  with respect to the 15° inclination. The deviation in average  $TKE$  is even smaller, around 4%. Similar results can be observed in Case B-2 with gradients instead of a flat terrain: the absolute percentage deviation is less than 5% for averaged wind  $VR$  and less than 8% for average  $TKE$ . However, the percentage difference becomes unsatisfactory in both averaged  $VR$  and  $TKE$  when the inclination of the buffer area is set to 90° for cases with either flat or hilly terrains. Relative to the cases with a 15° inclination, the absolute percentage difference for the 90° inclination in cases with non-flat topographies reaches more than 60% in averaged wind and greater than 100% in averaged  $TKE$ .

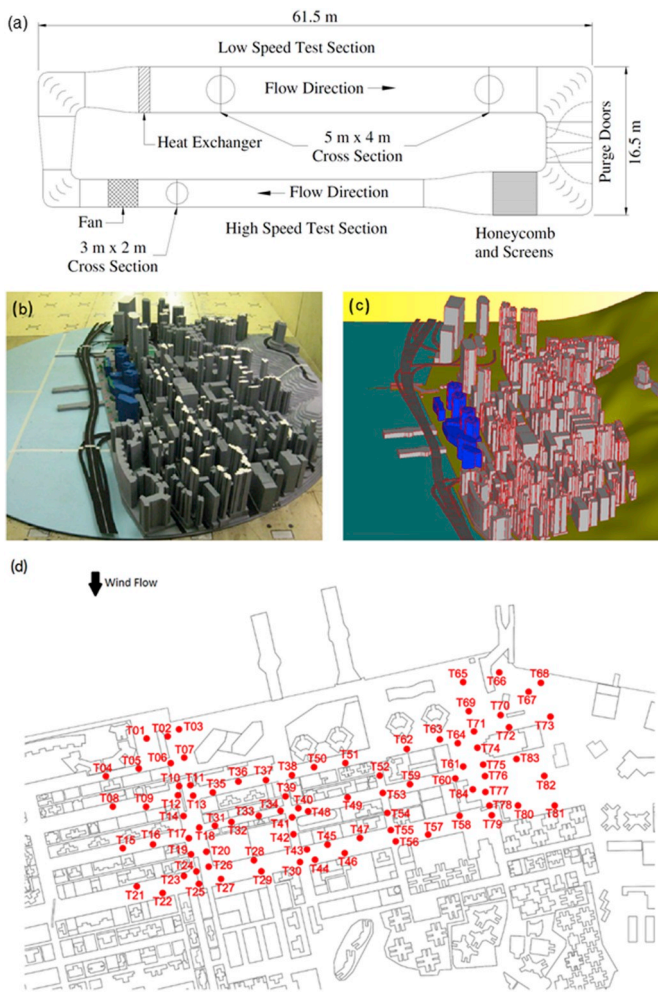


Fig. 6. Illustration of the (a) cross section of wind tunnel (b) modeled urban geometry - wind tunnel experiment (c) modeled urban geometry - CFD simulation (d) top view with test point locations.

From the above findings, it can be concluded that a 30° inclined buffer area can produce satisfactory and robust results (in both trends and magnitude) relative to cases with 15° inclined buffer areas. Any cases with buffer area inclinations beyond 30° produce undesirable simulation results. Therefore, when adopting Approach B with a buffer

**Table 2**  
Settings for the CFD simulations of the cases.

	Settings for CFD models
Boundary conditions	Symmetry conditions for the two sides and top boundary Wall boundary condition for the buildings and ground Velocity inlet condition for the inflow boundary Outflow condition for the outlet boundary
Turbulence model	Realizable $k - \epsilon$ model
Wall function	Standard wall function
Numerical scheme for pressure term and advection terms	Second-order for the pressure term Second-order upwind schemes for advection terms
Prismatic layers	Around all wall faces including buildings
Convergence Criteria	Scaled residuals reduced to below $1 \times 10^{-4}$

**Table 3**  
Settings for the CFD simulation of the validation case.

Test cases	Domain dimensions ( $H_T = 0.5m$ , tallest building height)	Approximate number of grid points
Case D-1	$R_i = 3H_T, R_l = 0.1H_T, R_o = 0.1H_T, H_D = 15H_T$	5.3 million
Case D-2	$R_i = 15H_T, R_l = 10H_T, R_o = 15H_T, H_D = 15H_T$	8 million
Case D-3	$R_i = 3H_T, R_l = 0.1H_T, R_o = 0.1H_T, D_i = 15R_i, D_l = 15R_l, D_o = 33R_l, H_D = 15H_T$	8.4 million
Case D-4	$R_i = 15H_T, R_l = 10H_T, R_o = 15H_T, D_i = 7R_l, D_l = 7R_l, D_o = 20R_l, H_D = 15H_T$	9 million

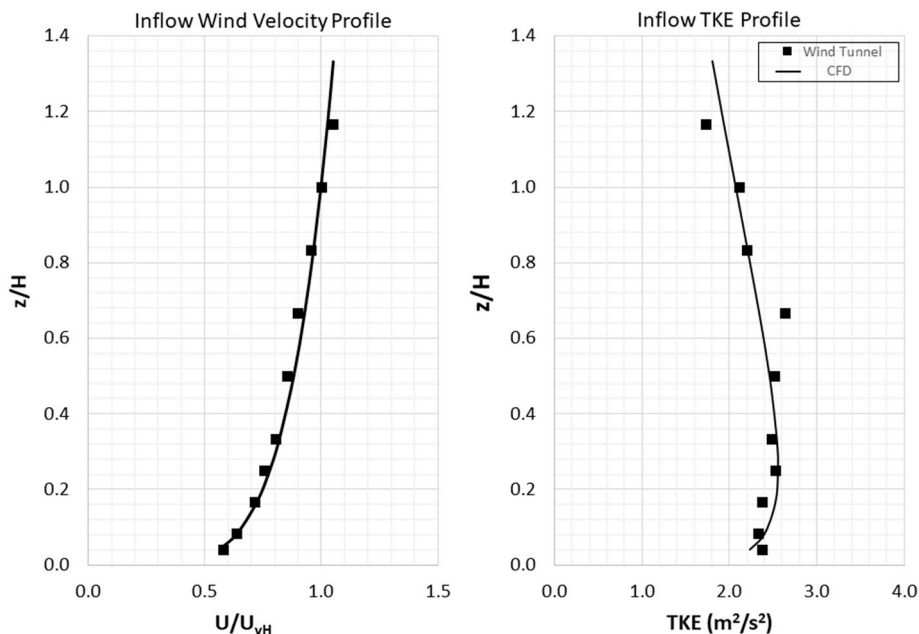


Fig. 7. Fitted inflow profiles for CFD validation based on wind tunnel data from “Final report for an instructed project at ex-North Point estate site – WWTF investigation report WWTF015-2008”.

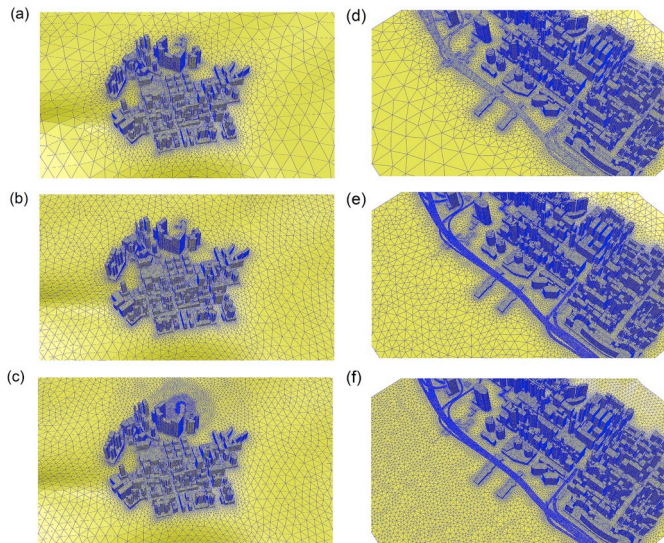


Fig. 8. Illustrations of coarse, basic and fine grids for (a–c) Case B-2/Case C-3B (d–f) Case D-3.

area in CFD simulations of wind environments, the inclination angle of the buffer area should be set to a maximum of  $\theta = 30^\circ$ .

6.2. Sensitivity to terrain size in two simulation approaches (Cases C)

This section investigates the influence of terrain size on the predicted wind and turbulence quantities within the same dense urban area under the two terrain modeling approaches. The cases start from a terrain size

of  $R = 500m$  from the simulated city edge and increase at  $500m$  increments until  $4R = 2000m$ .

Contours of wind velocity ratio and absolute difference in wind velocity ratio between various cases are also provided in Fig. 14. Owing to the similar in nature of the wind velocity ratio contours for the series of Cases C using Approach A and Approach B, aiming to avoid redundancy, only contours for selective cases were presented here. Fig. 15 contains bar charts showing the cross comparisons of pedestrian wind velocity ratio within the simulated urban area among all Cases C.

No simulation results were obtained for Case C-1A, because this case was obliged to be modeled with a very small computational domain, resulting in short distances from the geometric edges of the urban area to the domain boundaries, causing numerical divergence. Observable variances in wind velocity ratio values were discovered at majority upwind test points located within Group 4 and Group 5 (i.e., Test Points T33 to T49) for Cases C-2A to C-4A, while a good agreement in wind velocity ratio was reached among the cases at downwind test point locations (i.e. Test Points T1 to T20). This finding can be better observed from the contour plots displaying the absolute wind VR differences at pedestrian level between Cases C-2A/C-3A and Cases C-3A/C-4A in Fig. 14a and b, respectively. Similar features can also be seen among cases adopting Approach B (Cases C-1B to C-4B). The contour plot in Fig. 14c reflected the discrepancies in pedestrian wind velocity ratio across Cases C-3B and C-4B with different terrain extents were more observable for certain upwind test points in Group 3 (i.e., Test Points T26 to T28), Group 4 (i.e., T33, T35 to T38) and Group 5 (i.e., T39, T43 to T46 and T49) compared to those downwind test points within Group 1 and Group 2. The comparative contour plots in Fig. 14e and f demonstrated the predicted wind patterns near/within the simulated urban area for Cases C-3A and C-4A.

It can be seen from the contours that the two cases displayed a broad

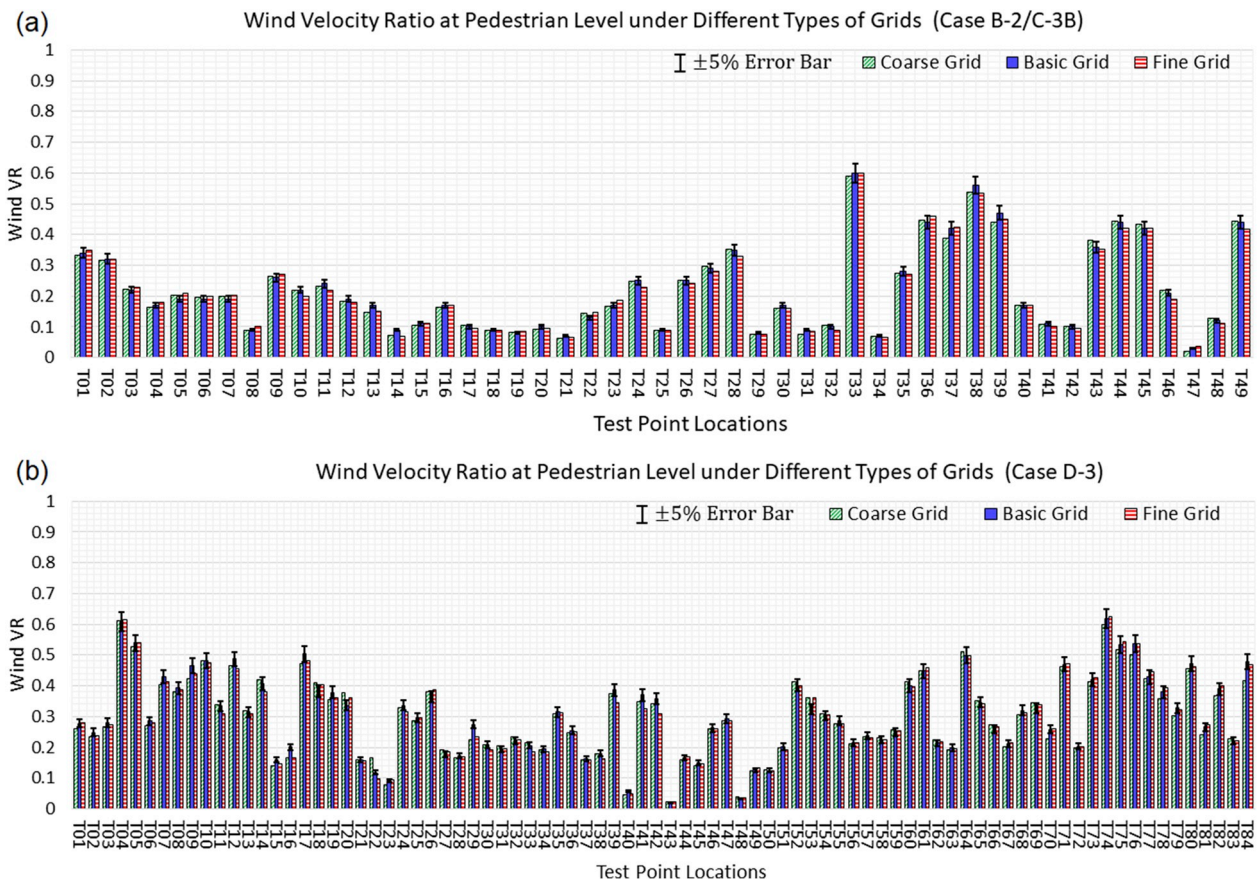


Fig. 9. Bar charts of pedestrian wind VR at various test point locations for (a) Case B-2/C-3B (b) Case D-3 under different computational grid resolutions.

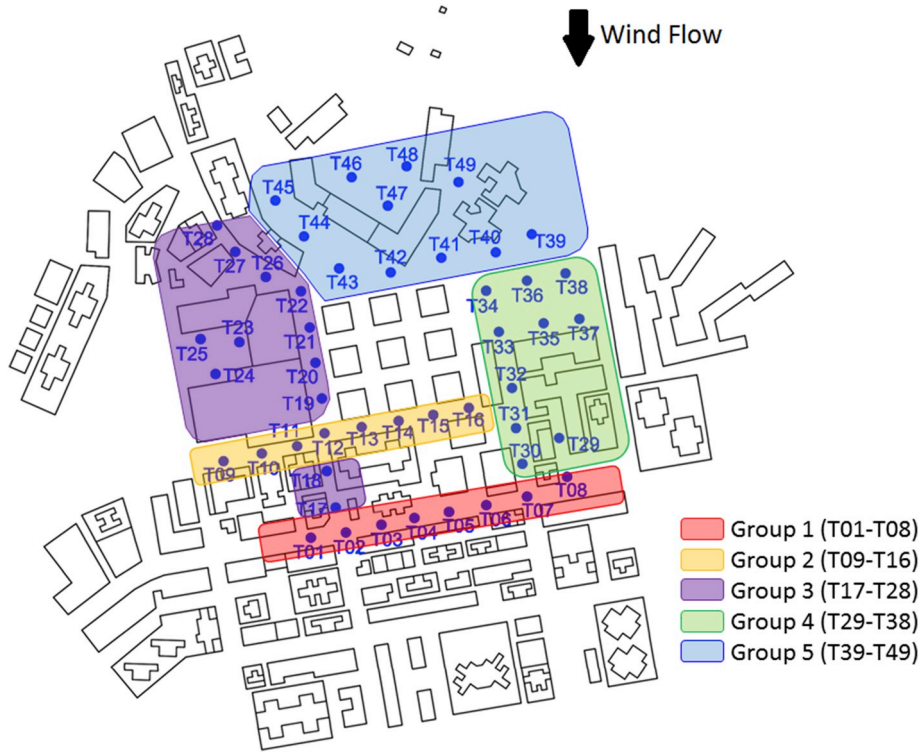


Fig. 10. Test point locations/groupings and geometry design for Cases A, B, and C.

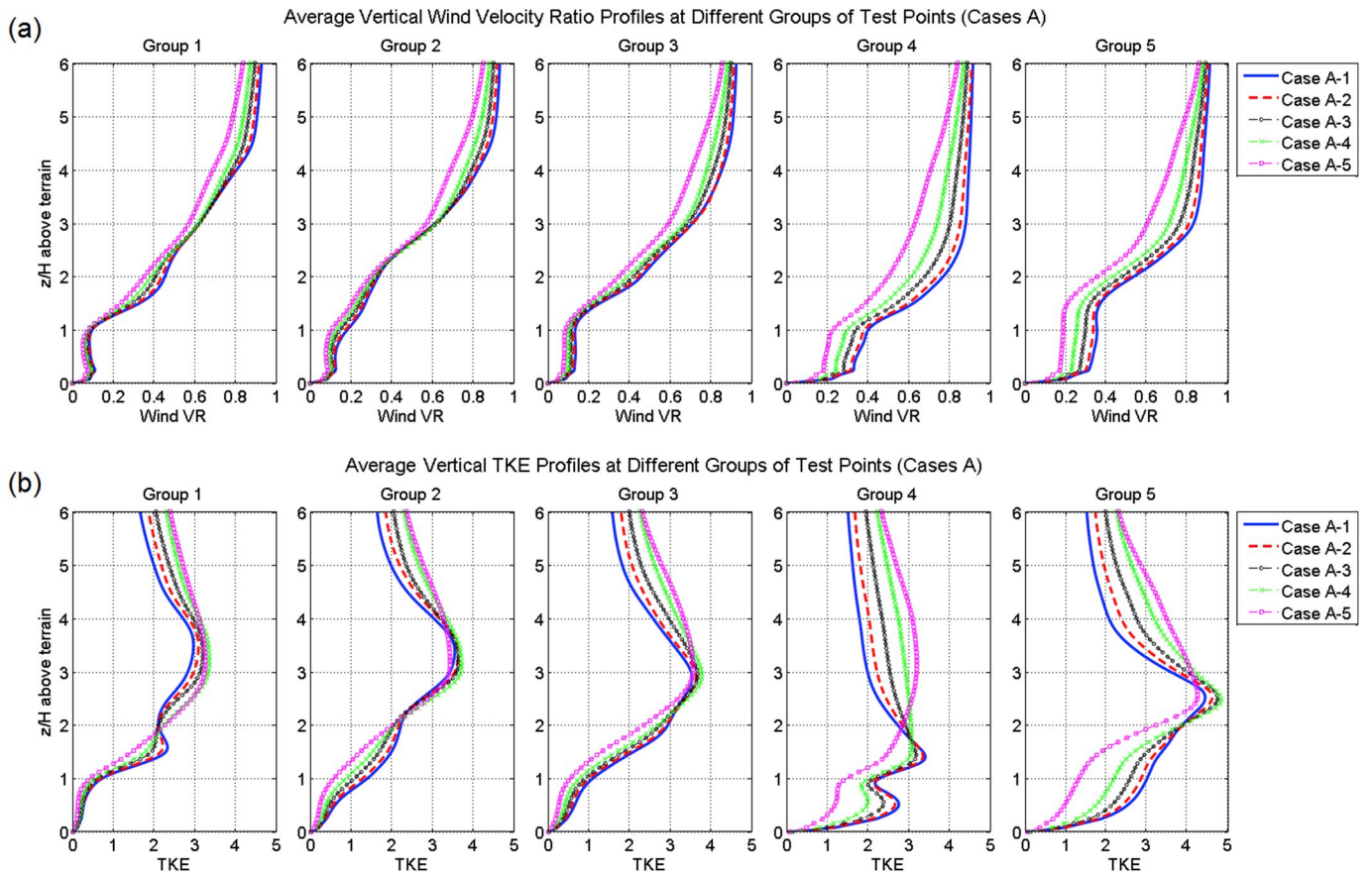


Fig. 11. Average vertical profiles of (a) wind velocity ratio and (b) turbulent kinetic energy for different groups of test points for Cases A.

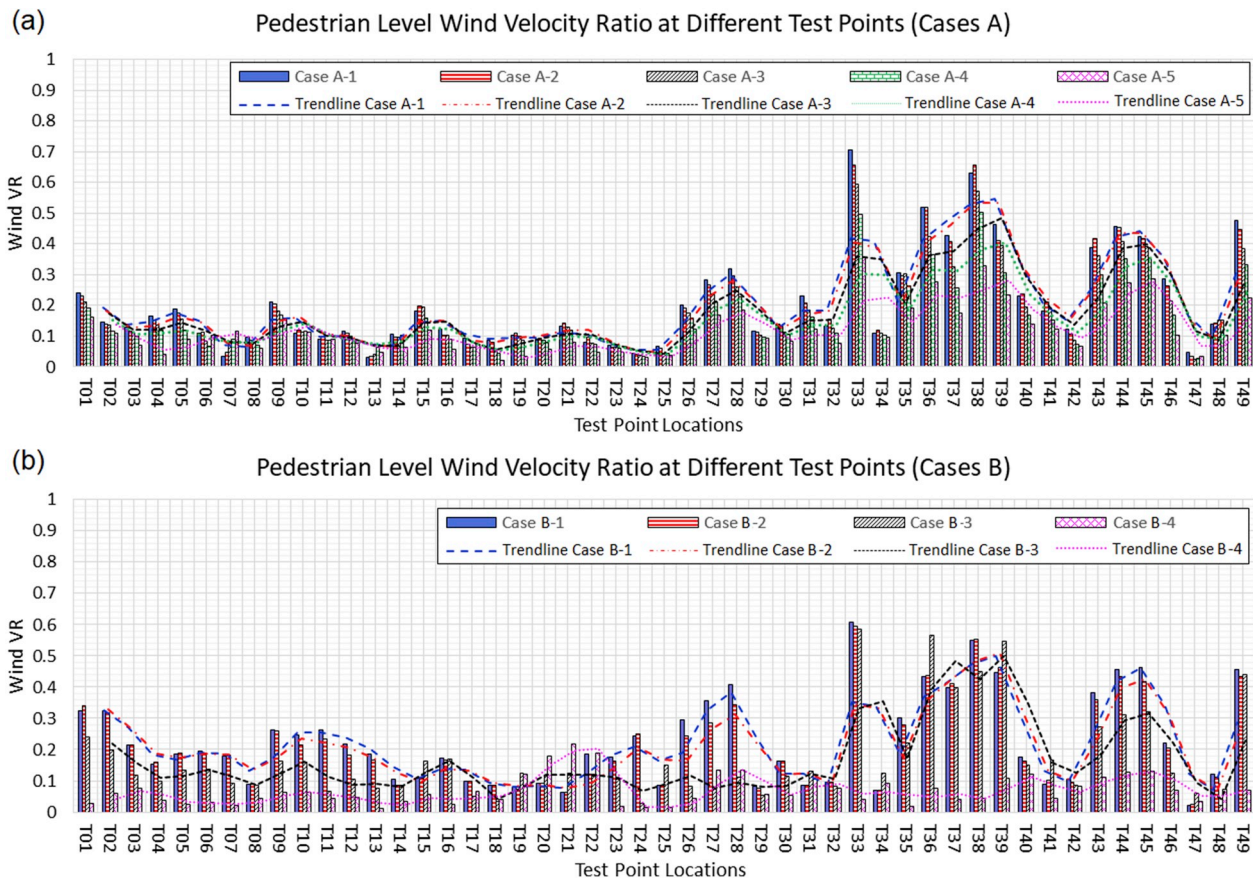


Fig. 12. Comparison of wind velocity ratio at pedestrian level for (a) Cases A (b) Cases B.

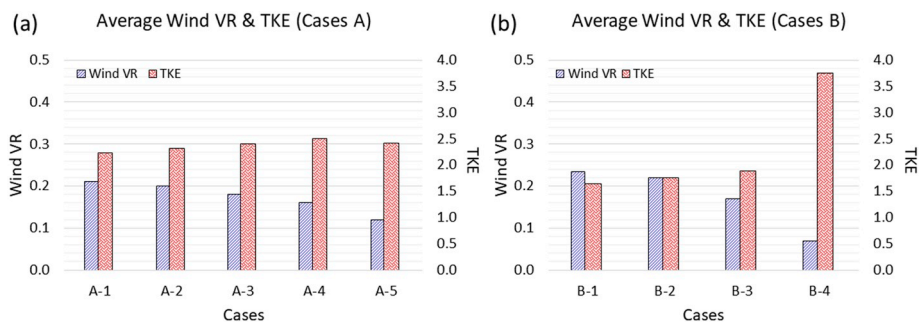


Fig. 13. Average wind velocity ratio and turbulent kinetic energy for (a) Cases A and (b) Cases B.

similarity in predicted pedestrian wind flow patterns (i.e., predicted locations within the city where high or low pedestrian wind velocity ratio occurred were consistent among the cases) within the simulated city but with greater differences at locations surrounding it. The possible explanation for the aforementioned observations is that the simulated wind flow pattern and the magnitudes of pedestrian wind velocity ratio at the upwind surrounding regions of the urban city are relatively more sensitive to the topological features/extents of the modeled terrain, while the wind at relatively downwind region within the urban city is predominantly affected by the building morphologies rather than topographic features.

In addition, Fig. 14d shows the absolute differences in wind velocity ratio for Cases C-4A and C-4B with a consistent terrain extent but different terrain treatment techniques. From this contour, it can be implied that there would also be spatial differences of predicted pedestrian wind velocity ratio magnitude within and at the near surrounding of the simulated urban city with the adoption of different

terrain modelling approaches.

The average pedestrian wind and turbulent kinetic energy data from the simulated cases are presented in Fig. 16. The results indicate that the predicted averaged VR values vary according to the terrain extent under both terrain treatment approaches. This implies that the predicted magnitudes of averaged pedestrian wind VR within an urban area will be affected whenever the extent of the modeled terrain changes.

The average pedestrian wind VR and TKE values with the two terrain modeling approaches are shown in Table 5, grouped according to the modeled terrain size. Approach B generally offers similar predictions of pedestrian wind magnitude and average TKE to those simulated via Approach A under the same terrain size, with average relative percentage differences of approximately 15%, for the two variables.

From these findings, it is suggested that although similar trends of wind behavior were predicted regardless of the terrain extent under the various scenarios, the variation in the modeled terrain size can be expected to have certain impacts on the predicted magnitude of the wind

**Table 4**  
Summary of CFD simulation results for Cases A and Cases B.

Test cases	$VR_{average}$	Absolute % difference of $VR_{average}$ (Relative to the case with 15° inclination)	$TKE_{average}$ (m <sup>2</sup> /s <sup>2</sup> )	Absolute % difference of $TKE_{average}$ (Relative to the case with 15° inclination)
Case A-1	0.21	–	2.23	–
Case A-2	0.20	4.8%	2.32	4.0%
Case A-3	0.18	14.3%	2.40	7.6%
Case A-4	0.16	23.8%	2.51	12.6%
Case A-5	0.12	42.9%	2.41	8.1%
Case B-1	0.23	–	1.64	–
Case B-2	0.22	4.3%	1.76	7.3%
Case B-3	0.17	26.1%	1.89	15.2%
Case B-4	0.07	69.6%	3.75	>100%

at pedestrian level and also the level of turbulence. Moreover, the results indicate there are certain differences in the magnitude of results predicted via the two approaches.

To identify which of the two approaches gives better and robust results, the results predicted from CFD simulations on a dense urban area generated by the two approaches are validated and compared with wind tunnel data in the next section.

### 6.3. Validation results

Having established an appropriate way to model the buffer area in Approach B through the insights from the simulations of Cases A and B and having investigated the influence of terrain size on the wind environment within the simulated dense city calculated by the two approaches in Cases C. This section addresses which of the two approaches provides better simulation robustness and flexibility. To this end, the CFD simulation results from Cases D will be compared with a set of wind tunnel data measured at various locations under the prevailing northerly wind.

The building geometries in all the Cases D were constructed as close to those in the wind tunnel as possible. However, consistent computational domain topology as in the wind tunnel experiment cannot be maintained with the adoption of Approach A in Cases D-1 and D-2. Fig. 15a compares the simulated wind velocity ratios of various Cases D with the wind tunnel data measured at the locations presented in Fig. 13c. Wind tunnel data at 84 locations (all at the pedestrian level 2m above ground) were compared with the CFD simulation results.

As seen in Fig. 17a, no simulation data are given for Case D-1. This is because the close proximity between the city and the domain boundary hindered the development of the inflow profiles and the recovery of the downwind wakes while creating artificial acceleration at the edges of buildings, which resulted in the numerical divergence of the simulation despite the use of numerical smoothing techniques.

To ensure that Approach A could be successfully adopted in the CFD simulation, a mitigation case (Case D-2) was constructed by enlarging

the terrain extent. In addition, Case D-4, adopting Approach B with the same terrain extent in Case D-2 and also consistent domain topology as the wind tunnel, was developed to provide reference comparison. As revealed from the results in Section 6.2, the size of the topographic features included in the model would affect the wind velocity ratios within the dense urban area. This is clearly reflected by the averaged wind velocity ratios of the results for Case D-2 (0.23) and Case D-4 (0.28), which are both under-predicted relative to the value from the wind tunnel experiment (0.34). Nevertheless, due to the consistency in computational domain topology with the wind tunnel, Case D-4, which used Approach B, more closely reproduced the averaged wind VR from the wind tunnel data than Case D-2, which adopted Approach A.

Although the average wind VR obtained from Case D-3 was still under-predicted relative to the wind tunnel data, this case, with the closest geometric similarity to the wind tunnel experiment, most accurately reproduced the wind VR value (0.30) from the physical experiment among all Cases D. Although Case D-3 produced relatively satisfactory simulation results, at certain test point locations (e.g., T31 to T34) the wind VR values were observably under-predicted relative to the experimental data. Test points T31 to T34 are located within the street canyon and are potentially sheltered by tall buildings against the northerly wind. One potential explanation for the relatively high wind velocity ratio measured at these test points is measurement error during the wind tunnel experiment.

Willemsen [96] reported that wind tunnel experiments could be conservatively estimated to have a standard measurement error of 20% for the pedestrian-level wind. Therefore, it should be noted that wind tunnel data must also include a certain amount of uncertainty. However, many other uncertain factors include but are not limited to the discrepancies that arise from the simplification of the modeled geometries/topography/buffer areas, inflow atmospheric conditions, model parameter settings, and choices of turbulence models [84,97–105], presumably would contribute to the deviation of the CFD results from the wind tunnel measurements.

In addition to the average VR, values of three other validation metrics are summarized in Table 6. Simulation results from Case D-3 have the best correlation with the wind tunnel data (see Fig. 17c), the lowest value of NMSE, and the highest FAC2 value. Case D-4 has a lower NMSE and a higher FAC2 than Case D-2 but a similar correlation. These results show that Case D-3 outperforms Cases D-2 and D-4 in terms of simulation robustness in the prediction of the wind velocity ratio. Furthermore, strong evidence shows that modeling Approach B, which incorporates a buffer area, provides greater flexibility and performs better than Approach A, in which the terrain covers the entire ground of the computational domain.

## 7. Conclusions

More than a decade has passed since the launch of the AVA system in Hong Kong. The use of CFD in these kinds of assessments has become common in the environmental industries. However, many AVA reports still seem to lack technical details and use a wide range of model simulation settings. One reason behind this is the lack of informative guidelines relating to CFD model settings incorporated into the issued AVA Technical Circular upon the launch of the AVA system.

There is a growing tendency for the environmental consultancy industry to extend the use of CFD from AVA applications to other environmental assessments, which include but are not limited to indoor/outdoor pollutant dispersion simulations and thermal comfort simulations [30,49]. This paper reviewed and summarized the main aspects of the best practice guidelines for CFD modeling, anticipating an enriched and more detailed circular that would result in better usage of the CFD tool by the consultancy industry.

After revisiting the existing guidelines, this study focused on the aspect of terrain modeling under two major approaches. Twenty-one cases were investigated with the realizable  $k-\epsilon$  model and were

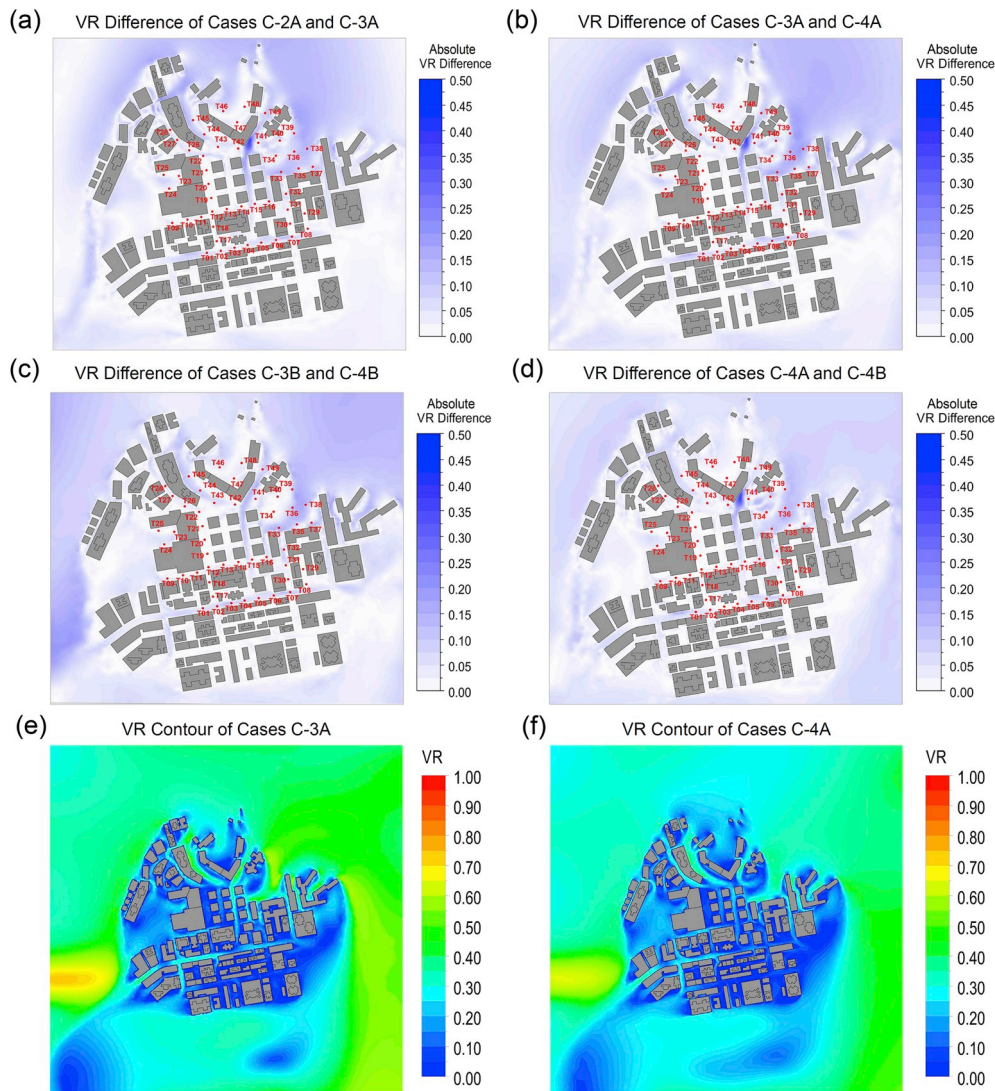


Fig. 14. Contours of absolute wind velocity ratio difference and wind velocity ratios for selective Cases C at pedestrian level.

categorized into four series: Cases A, B, C and D. Under a fixed terrain size, Cases A and B were simulated to systematically establish the most appropriate inclination angle  $\theta$  of the buffer area in Approach B. Using both terrain treatment approaches, Cases C were run to demonstrate the effect of the modeled terrain size on the pedestrian wind environment and turbulent kinetic energy within the modeled city. Following Cases A to C, simulations were carried out, again with both terrain treatment approaches, for Cases D and inter-compared with wind tunnel results to validate not only the appropriateness of the two modeling approaches but also the performance of the turbulence model. The results reveal the following key insights and conclusions.

- Under Approach B, a smaller inclination angle  $\theta$  is preferred for buffer areas that connect the computational boundaries and the topographical features. Larger inclination angles result in greater deviation of the predicted values for pedestrian wind and turbulence quantities. To ensure robustness, a  $\theta$  value of  $30^\circ$  or less for the buffer area is required when adopting Approach B for CFD simulations of AVA projects.
- Except for specific cases in which a change in terrain size would filter out observable topographical features, in general, minor alterations in the extent of terrain in CFD simulations do not greatly influence the wind distribution within a dense urban area. However, such

adjustments cause certain changes in the magnitude of the simulated pedestrian wind and turbulence quantities.

- Although being a relatively direct and simple method for modeling terrain features, Approach A encountered difficulties in numerical convergence when the topographical extents were limited. In such cases (Case C-1A and Case D-1), the modeled geometries were bounded within a very small computational domain, leading to short distances between the edges of the building geometries and the boundaries of the domain. This finding implies that Approach A is only applicable if the terrain features involved in the simulations have sufficient size.

A comparison of the simulated results with the data from wind tunnel experiments shows that the agreement between the simulation models and the physical experiments in terms of the pedestrian wind velocity ratio was better for Approach B. The findings suggest that a terrain modeling method that incorporates a buffer area (Approach B) performs better than the approach in which terrain features cover the entire ground of the computational domain (Approach A).

To summarize, Approach B performs better than Approach A not only in terms of robustness in simulation results but also in terms of ease in numerical convergence. Moreover, Approach B, with an inclined buffer area, is able to bypass the constraint against enlarging the terrain to achieve numerical convergence, which afflicts Approach A.

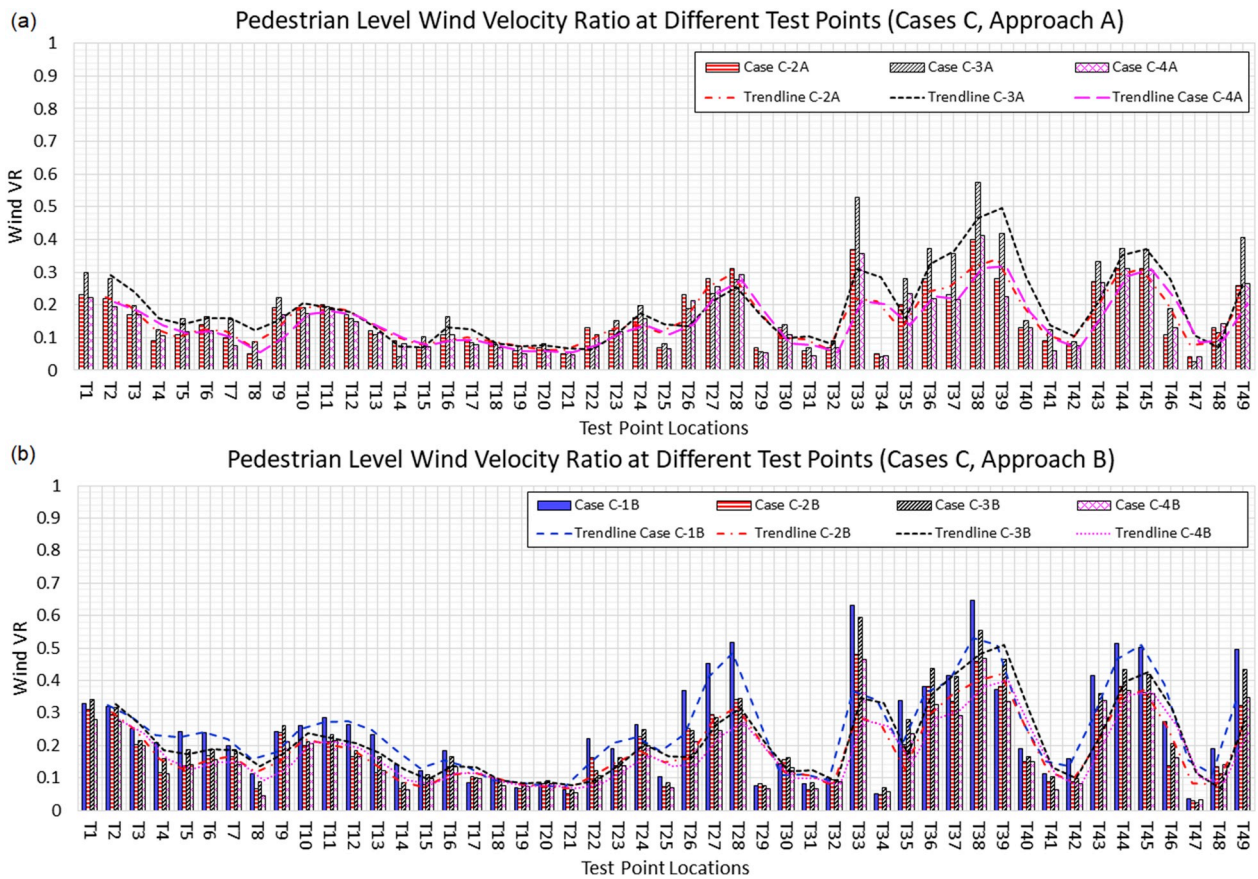


Fig. 15. Comparison of wind velocity ratio at pedestrian level for Cases C modeled via (a) Approach A and (b) Approach B.

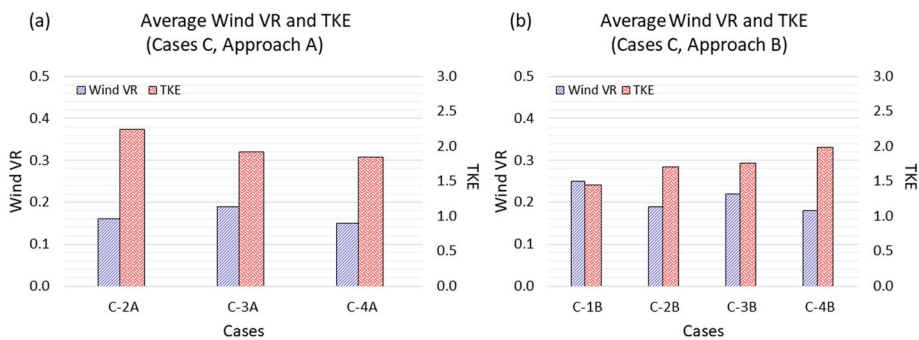


Fig. 16. Average wind velocity ratio and turbulent kinetic energy for Cases C modeled through (a) Approach A and (b) Approach B.

Table 5  
Summary of CFD simulation results for Cases C.

Test cases	$VR_{avg}$	Relative %Δ of $VR_{average}$ $100\% \times \frac{ VR_{avg-A} - VR_{avg-B} }{\max(VR_{avg-A}, VR_{avg-B})}$	$TKE_{avg}(m^2/s^2)$	Relative %Δ of $TKE_{average}$ $100\% \times \frac{ TKE_{avg-A} - TKE_{avg-B} }{\max(TKE_{avg-A}, TKE_{avg-B})}$
Case C-1A	–	–	–	–
Case C-1B	0.25	–	1.45	–
Case C-2A	0.16	15.8%	2.24	23.7%
Case C-2B	0.19	–	1.71	–
Case C-3A	0.19	13.6%	1.92	8.3%
Case C-3B	0.22	–	1.76	–
Case C-4A	0.15	16.7%	1.84	7.5%
Case C-4B	0.18	–	1.99	–

However, under the current AVA system for putting forward developments in Hong Kong, without a wind performance criterion, the approval criteria are based on a comparison of average pedestrian wind

velocity ratios predicted from CFD simulations of a wide range of development scenarios. Under the current practice, provided that the comparative simulations were carried out on a fair basis (i.e., a

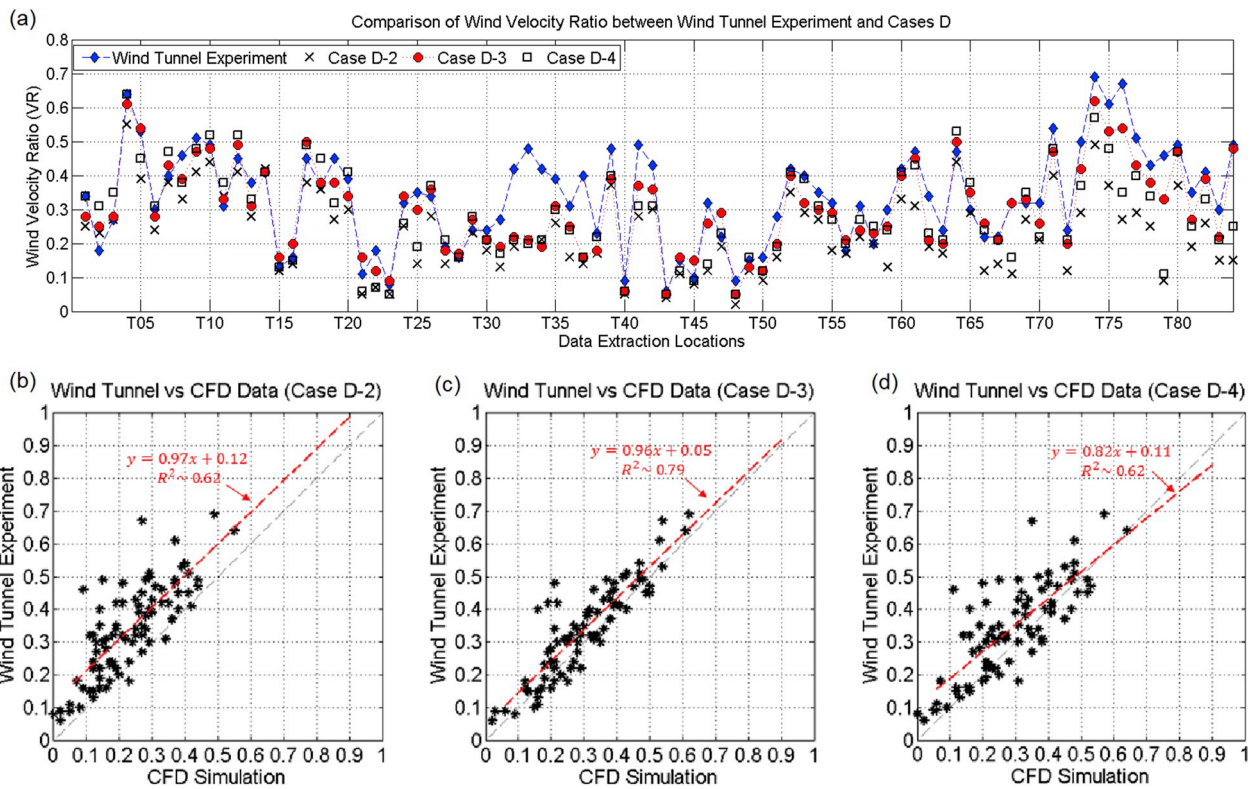


Fig. 17. Wind tunnel experiment against CFD simulation results (a) pedestrian level test points (b) Case D-2 (c) Case D-3 (d) Case D-4.

Table 6

Summary of average wind velocity ratio, NMSE, FAC2 and correlation for Cases D against wind tunnel experiment.

Test cases	$VR_{average}$	NMSE	FAC2	Correlation value
Case D-1	–	–	–	–
Case D-2	0.23	0.25	0.79	0.62
Case D-3	0.30	0.05	0.94	0.79
Case D-4	0.28	0.11	0.89	0.62

consistent approach, appropriate model settings following the suggestions in this paper, consistent choice of turbulence models, etc.), the adoption of either of the approaches to terrain treatment discussed in this study would not lead to a wrong decision to be made. Finally, care must be taken to ensure numerical convergence, typically monitored by scaled residuals, for any numerical simulations.

**Declaration of competing interest**

The authors declare that they have no known competing financial interests or personal relationships that could have appeared to influence the work reported in this paper.

**Acknowledgments**

This work was supported by the Air Pollution Control Program of the National Key Research and Development Plan (2018YFC0213902), the Environment and Conservation Fund (ECWW19IP03) and RGC Research Impact Fund (R4046-18). The authors would like to thank the anonymous reviewers for their useful suggestions.

**References**

- [1] HKPD (Hong Kong Planning Department), Feasibility Study for Establishment of Air Ventilation Assessment System, Final Report, The government of the Hong Kong Special Administrative Region, 2005.
- [2] HKPD (Hong Kong Planning Department), Hong Kong Planning Standards and Guidelines, The government of the Hong Kong Special Administrative Region, 2006.
- [3] HKPD (Hong Kong Planning Department), Urban Climatic Map and Standards for Wind Environment - Feasibility Study Final Report, The government of the Hong Kong Special Administrative Region, 2012.
- [4] E. Ng, Designing for thermal comfort and air ventilation in high density city conditions - air ventilation assessment system (AVAS), HKIA J (2007) 24–31.
- [5] E. Ng, Policies and technical guidelines for urban planning of high-density cities - air ventilation assessment (AVA) of Hong Kong, Build. Environ. 44 (7) (2009) 1478–1488.
- [6] Hong Kong Housing, Planning, Lands, Environment, Transport and Works Bureau, The government of the Hong Kong Special Administrative Region, 2006. Technical Circular No. 1/06 Air Ventilation Assessment.
- [7] J.J. Baik, R.S. Park, H.Y. Chun, J.J. Kim, A Laboratory model of urban street canyon flows, J. Appl. Meteorol. 39 (2000) 1592–1600.
- [8] A. Robins, Wind tunnel dispersion modelling some recent and not so recent achievements, J. Wind Eng. Ind. Aerodyn. 91 (2003) 1777–1790.
- [9] K. Ahmad, M. Khare, K.K. Chaudhry, Wind tunnel simulation studies on dispersion at urban street canyons and intersections: a review, J. Wind Eng. Ind. Aerodyn. 93 (2005) 697–717.
- [10] I. Mavroidis, R.F. Griffiths, D.J. Hall, Field and wind tunnel investigations of plume dispersion around single surface obstacles, Atmos. Environ. 37 (21) (2003) 2903–2918.
- [11] C.R. Wood, J.F. Barlow, S.E. Belcher, A. Dobre, S.J. Arnold, A.A. Balogun, J.J. N. Lingard, R.J. Smalley, J.E. Tate, A.S. Tomlin, R.E. Britter, H. Cheng, D. Martin, F.K. Petersson, D.E. Shallcross, I.R. White, M.K. Neophytou, A.G. Robins, Dispersion experiments in central london: the 2007 DAPPLE project, Bull. Am. Meteorol. Soc. 90 (2009) 955–969.
- [12] P.Y. Cui, Z. Li, W.Q. Tao, Wind-tunnel measurements for thermal effects on the air flow and pollutant dispersion through different scale urban areas, Build. Environ. 97 (2016) 137–151.
- [13] A. Baskaran, A. Kashef, Investigation of air flow around buildings using computational fluid dynamics techniques, Eng. Struct. 18 (1996) 861–873, 75.
- [14] B. Blocken, J. Persoon, Pedestrian wind comfort around a large football stadium in an urban environment: CFD simulation, validation and application of the new Dutch wind nuisance standard, J. Wind Eng. Ind. Aerodyn. 97 (2009) 255–270.
- [15] T. Van Hooff, B. Blocken, On the effect of wind direction and urban surroundings on natural ventilation of a large semi-enclosed stadium, Comput. Fluids 39 (2010) 1146–1155.

- [16] B. Blocken, J. Carmeliet, T. Stathopoulos, Application of computational fluid dynamics in building performance simulation for the outdoor environment: an overview, *J. Build. Perform. Simulat.* 4 (2010) 157–184.
- [17] Z.L. Gu, Y.W. Zhang, Y. Cheng, S.C. Lee, Effect of uneven building layout on air flow and pollutant dispersion in non-uniform street canyons, *Build. Environ.* 46 (2011) 2657–2665.
- [18] W.D. Janssen, B. Blocken, T. van Hooff, Pedestrian wind comfort around buildings: comparison of wind comfort criteria based on whole-flow field data for a complex case study, *Build. Environ.* 59 (2013) 547–562.
- [19] E. Yasa, Computational evaluation of building physics - the effect of building form and settled area, microclimate on pedestrian level comfort around buildings, *Build. Simulat.* 9 (2016) 489–499.
- [20] Y.H. Juan, A.S. Yang, C.Y. Wen, Y.T. Lee, P.C. Wang, Optimization procedures for enhancement of city breathability using arcade design in a realistic high-rise urban area, *Build. Environ.* 121 (2017) 247–261.
- [21] S. Liu, W. Pan, H. Zhang, X. Cheng, Z. Long, Q. Chen, CFD simulations of wind distribution in an urban community with a full-scale geometrical model, *Build. Environ.* 117 (2017) 11–23.
- [22] C. Wen, Y. Juan, A. Yang, Enhancement of city breathability with half open spaces in ideal urban street canyons, *Build. Environ.* 112 (2017) 322–336.
- [23] A.Z. Dhunny, N. Samkhaniani, M.R. Lollchund, S.D.D.V. Rughooputh, Investigation of multi-level wind flow characteristics and pedestrian comfort in a tropical city, *Urban Clim* 24 (2018) 185–204.
- [24] Y. Du, C.M. Mak, Z. Ai, Modelling of pedestrian level wind environment on a high-quality mesh: a case study for the HKPolyU campus, *Environ. Model. Softw* 103 (2018) 105–119.
- [25] L. Peng, J.P. Liu, Y. Wang, P. Chan, T. Lee, F. Peng, M. Wong, Y. Li, Wind weakening in a dense high-rise city due to over nearly five decades of urbanization, *Build. Environ.* 138 (2018) 207–220.
- [26] K. An, S.M. Wong, J.C.H. Fung, Exploration of sustainable building morphologies for effective passive pollutant dispersion within compact urban environments, *Build. Environ.* 148 (2019) 508–523.
- [27] S.R. Hanna, M.J. Brown, F.E. Camell, S.T. Chan, W.J. Coirier, O.R. Hansen, A. H. Huber, S. Kim, R.M. Reynolds, Detailed simulations of atmospheric flow and dispersion in downtown Manhattan: an application of five computational fluid dynamics models, *Bull. Am. Meteorol. Soc.* 87 (2006) 1713–1726.
- [28] M. Lateb, C. Masson, T. Stathopoulos, C. Bedard, Numerical simulation of pollutant dispersion around a building complex, *Build. Environ.* 45 (2010) 1788–1798.
- [29] M. Lateb, C. Masson, T. Stathopoulos, C. Bedard, Effect of stack height and exhaust velocity on pollutant dispersion in the wake of a building, *Atmos. Environ.* 45 (2011) 5150–5163.
- [30] B. Blocken, Y. Tominaga, T. Stathopoulos, CFD simulation of micro-scale pollutant dispersion in the built environment, *Build. Environ.* 64 (2013) 225–230.
- [31] N. Antoniou, H. Montazeri, H. Wigo, M. Neophytou, B. Blocken, M. Sandberg, CFD and wind-tunnel analysis of outdoor ventilation in a real compact heterogeneous urban area: evaluation using “air delay”, *Build. Environ.* 126 (2017) 355–372.
- [32] R.N. Meroney, M. Pavageau, S. Rafailidis, M. Schatzmann, Study of line source characteristics for 2-D physical modelling of pollutant dispersion in street canyons, *J. Wind Eng. Ind. Aerodyn.* 62 (1996) 37–56.
- [33] A.T. Chan, E.S.P. So, S.C. Samad, Strategic guidelines for street canyon geometry to achieve sustainable street air quality, *Atmos. Environ.* 35 (32) (2001) 5681–5691.
- [34] A.P.G. Sagrado, J. Van Beeck, P. Rambaud, D. Olivari, Numerical and experimental modelling of pollutant dispersion in a street canyon, *J. Wind Eng. Ind. Aerodyn.* 90 (2002) 321–339.
- [35] V.D. Assimakopoulos, H.M. ApSimon, N. Moussiopoulos, Numerical study of atmospheric pollutant dispersion in different two-dimensional street canyon configurations, *Atmos. Environ.* Times 37 (2003) 4037–4049.
- [36] C.H. Liu, D.Y.C. Leung, M.C. Barth, On the prediction of air and pollutant exchange rates in street canyons of different aspect ratios using large-eddy simulation, *Atmos. Environ.* 39 (2005) 1567–1574.
- [37] X. Xie, Z. Huang, J. Wang, The impact of urban street layout on local atmospheric environment, *Build. Environ.* 41 (10) (2006) 1352–1363.
- [38] X.X. Li, C.H. Liu, D.Y.C. Leung, Large-eddy simulation of flow and pollutant dispersion in high-aspect-ratio urban street canyons with wall model, *Boundary-Layer Meteorol.* 129 (2) (2008) 249–268.
- [39] M. Chavez, B. Hajra, T. Stathopoulos, A. Bahloul, Near-field pollutant dispersion in the built environment by CFD and wind tunnel simulations, *J. Wind Eng. Ind. Aerodyn.* 99 (2011) 330–339.
- [40] B. Hajra, T. Stathopoulos, A. Bahloul, The effect of upstream buildings on near-field pollutant dispersion in the built environment, *Atmos. Environ.* 45 (2011) 4930–4940.
- [41] B. Hajra, T. Stathopoulos, A wind tunnel study of the effect of downstream buildings on near-field pollutant dispersion, *Build. Environ.* 52 (2012) 19–31.
- [42] Q.M.Z. Iqbal, A.L.S. Chan, Pedestrian level wind environment assessment around group of high-rise cross-shaped buildings: effect of building shape, separation and orientation, *Build. Environ.* 101 (2016) 45–63.
- [43] K. An, J.C.R. Hunt, J.C.H. Fung, Downwind flow behaviours of cuboid-shaped obstacles: modelling and experiments, *Proc. Inst. Civ. Eng. Comput. Mech.* 172 (1) (2019) 12–32.
- [44] J. Franke, C. Hirsch, A.G. Jensen, H.W. Krus, M. Schwartzman, P.S. Westbury, S. D. Miles, J.A. Wisse, N.G. Wright, Recommendations on the use of CFD in wind engineering, in: J.P.A.J. van Beek (Ed.), *Proc. Int. Conf. On Urban Wind Engineering and Building Aerodynamics: COST C14 – Impact of Wind and Storm on City Life and Built Environment*, 2004. Rhode-saint-geneve.
- [45] J. Franke, Recommendations of the COST action C14 on the use of CFD in predicting pedestrian wind environment, *J. Wind Eng.* 108 (2006) 529–532.
- [46] R. Britter, M. Schatzmann, *Model Evaluation Guidance and Protocol Document*, 2007. Available online, <http://www.cost.eu/media/publications/07-64-Model-Evaluation-Guidance-and-Protocol-Documnt>. (Accessed 8 January 2016).
- [47] Y. Tominaga, A. Mochida, R. Yoshie, H. Kataoka, T. Nozu, M. Yoshikawa, AIJ guidelines for practical applications of CFD to pedestrian wind environment around buildings, *J. Wind Eng. Ind. Aerodyn.* 96 (2008) 1749–1761.
- [48] B. Blocken, LES over RANS in building simulation for outdoor and indoor applications: a foregone conclusion? *Build. Simulat.* 11 (5) (2018) 821–870.
- [49] R. Alonso, M.G. Vivanco, I. Gonzalez-Fernandez, V. Bermejo, I. Palomino, J. L. Garrido, S. Elvira, P. Salvador, B. Artñano, Modelling the influence of peri-urban trees in the air quality of Madrid region (Spain), *Environ. Pollut.* 159 (2011) 2138–2147.
- [50] J. Franke, A. Hellsten, K. Schlunzen, B. Carissimo, Best Practice Guideline for the CFD Simulation of Flows in the Urban Environment. In the COST Action 732. Quality Assurance and Improvement of Meteorological Models, University of Hamburg, Meteorological Institute, Center of Marine and Atmospheric Sciences, 2007.
- [51] J. Franke, A. Hellsten, K. Schlunzen, B. Carissimo, The COST 732 best practice guideline for CFD simulation of flows in the urban environment: a summary, *Int. J. Environ. Pollut.* 44 (2011) 419–427.
- [52] J.H. Ferziger, Approaches to turbulent flow computation: applications to flow over obstacles, *J. Wind Eng. Ind. Aerodyn.* 35 (1990) 1–19.
- [53] M.A. Leschziner, Computational modelling of complex turbulent flow—expectations, reality and prospects, *J. Wind Eng. Ind. Aerodyn.* 46 (47) (1993) 37–51.
- [54] S. Murakami, Current status and future trends in computational wind engineering, *J. Wind Eng. Ind. Aerodyn.* 67 (68) (1997) 3–34.
- [55] A.D. Gosman, Developments in CFD for industrial and environmental applications in wind engineering, *J. Wind Eng. Ind. Aerodyn.* 81 (1999) 21–39.
- [56] R. Yoshie, A. Mochida, Y. Tominaga, H. Kataoka, K. Harimoto, T. Nozu, T. Shirasawa, Cooperative project for CFD prediction of pedestrian wind environment in the Architectural Institute of Japan, *J. Wind Eng. Ind. Aerodyn.* 95 (2007) 1551–1578.
- [57] C.J. Baker, Wind engineering—past, present and future, *J. Wind Eng. Ind. Aerodyn.* 95 (2007) 843–870.
- [58] W.C. Cheng, C.H. Liu, Y.C. Leung, Computational formulation for the evaluation of street canyon ventilation and pollutant removal performance, *Atmos. Environ.* 42 (2008) 9041–9051.
- [59] Z. Bu, S. Kato, Y. Ishida, H. Huang, New criteria for assessing local wind environment at pedestrian level based on exceedance probability analysis, *Build. Environ.* 44 (2009) 1501–1508.
- [60] J. Hang, M. Sandberg, Y. Li, Age of air and air exchange efficiency in idealized city models, *Build. Environ.* 44 (2009) 1714–1723.
- [61] J. Hang, M. Sandberg, Y. Li, Effect of urban morphology on wind condition in idealized city models, *Atmos. Environ.* 43 (2009) 869–878.
- [62] J. Hang, M. Sandberg, Y. Li, L. Claesson, Flow mechanisms and flow capacity in idealized long-street city models, *Build. Environ.* 45 (4) (2010) 1042–1053.
- [63] J. Hang, M. Sandberg, Y. Li, L. Claesson, Wind conditions and ventilation in high-rise long street models, *Build. Environ.* 45 (6) (2010) 1353–1365.
- [64] J. Hang, Y. Li, M. Sandberg, R. Buccolieri, S. Di Sabatino, The influence of building height variability on pollutant dispersion and pedestrian ventilation in idealized high-rise urban areas, *Build. Environ.* 56 (2012) 346–360.
- [65] J. Hang, Y. Li, M. Sandberg, R. Buccolieri, S. Di Sabatino, On the contribution of mean flow and turbulence to city breathability: the case of long streets with tall buildings, *Sci. Total Environ.* 416 (2012) 362–373.
- [66] J. Hang, Z. Luo, M. Sandberg, J. Gong, Natural ventilation assessment in typical open and semi-open urban environments under various wind directions, *Build. Environ.* 70 (2013) 318–333.
- [67] J. Hang, Y. Li, Ventilation strategy and air change rates in idealized high-rise compact urban areas, *Build. Environ.* 45 (2010) 2754–2767.
- [68] J. Hang, Y. Li, Wind conditions in idealized building clusters: macroscopic simulations using a porous turbulence model, *Bound-Layer Meteorol* 136 (2010) 129–159.
- [69] R. Buccolieri, M. Sandberg, S. Di Sabatino, City breathability and its link to pollutant concentration distribution within urban-like geometries, *Atmos. Environ.* 44 (2010) 1894–1903.
- [70] M. Pontiggia, M. Derudi, M. Alba, M. Scaioni, R. Rota, Hazardous gas releases in urban areas: assessment of consequences through CFD modelling, *J. Hazard Mater.* 176 (2010) 589–596.
- [71] M. Lin, J. Hang, Y. Li, Z. Luo, M. Sandberg, Quantitative ventilation assessments of idealized urban canopy layer with various urban layouts and the same building packing density, *Build. Environ.* 79 (2014) 152–167.
- [72] R. Ramponi, B. Blocken, L.B. de Coo, W.D. Janssen, CFD simulation of outdoor ventilation of generic urban configurations with different urban densities and equal and unequal street widths, *Build. Environ.* 92 (2015) 152–166.
- [73] M. Lateb, R.N. Meroney, M. Yataghene, H. Fellouah, F. Saleh, M.C. Boufadel, On the use of numerical modelling for near-field pollutant dispersion in urban environments - a review, *Environ. Pollut.* 208 (2016) 271–283 (Part A).
- [74] H. Yu, J. The, Validation and optimization of SST  $k-\omega$  turbulence model for pollutant dispersion within a building array, *Atmos. Environ.* 145 (2016) 225–238.

- [75] K. An, J.C.H. Fung, An improved SST  $k-\omega$  model for pollutant dispersion simulation within an isothermal boundary layer, *J. Wind Eng. Ind. Aerodyn.* 179 (2018) 369–384.
- [76] K. Hanjalic, Will RANS survive LES? A view of perspectives, *J. Fluids Eng.* 127 (2005) 831–839.
- [77] A. Mochida, Y. Tominaga, S. Murakami, R. Yoshie, T. Ishihara, R. Ooka, Comparison of various  $k-\epsilon$  models and DSM applied to flow around a high-rise building- report on ALJ cooperative project for CFD prediction of wind environment, *Wind Struct.* 5 (2002) 227–244.
- [78] V. Yakhot, S.A. Orszag, S. Thangam, T.B. Gatski, C.G. Speziale, Development of turbulence models for shear flows by a double expansion technique, *Phys. Fluids* 4 (7) (1992) 1510–1520.
- [79] T. Shih, W. Liou, A. Shabbir, J. Zhun, A new  $k-\epsilon$  eddy viscosity model for high Reynolds number turbulent flows - model development and validation, *Comput. Fluids* 24 (3) (1995) 227–238.
- [80] Evaluation of modelling uncertainty. CFD modelling of near-field atmospheric dispersion, in: R.C. Hall (Ed.), Project EMU Final Report, European Commission Directorate-General XII Science, Research and Development Contract EV5V-CT94-0531, WS Atkins Consultants Ltd., Surrey, 1997.
- [81] I.R. Cowan, I.P. Castro, A.G. Robins, Numerical considerations for simulations of flow and dispersion around buildings, *J. Wind Eng. Ind. Aerodyn.* 67–68 (1997) 535–545.
- [82] A. Scaperdas, S. Gilham, Thematic Area 4: best practice advice for civil construction and HVAC, The QNET-CFD Network Newsletter 2 (4) (2004) 28–33.
- [83] J.G. Bartzis, D. Vlachogiannis, A. Sfetsos, Thematic area 5: best practice advice for environmental flows, The QNET-CFD Network Newsletter 2 (4) (2004) 34–39.
- [84] K. An, J.C.H. Fung, S.H.L. Yim, Sensitivity of inflow boundary conditions on downstream wind and turbulence profiles through building obstacles using a CFD approach, *J. Wind Eng. Ind. Aerodyn.* 115 (2013) 137–149.
- [85] M. Casey, T. Wintergerste, ERCOFTAC Best Practice Guidelines: ERCOFTAC Special Interest Group on Quality and Trust in Industrial CFD, ERCOFTAC. Brussels, 2000.
- [86] Arup, Air Ventilation Assessment of Tonkin Street – Initial Study Report, Hong Kong Housing Authority, 2014. [https://www.pland.gov.hk/pland\\_en/info\\_serv/ava\\_register/ProjInfo/AVRG91\\_AVA\\_InitialStudyReport.pdf](https://www.pland.gov.hk/pland_en/info_serv/ava_register/ProjInfo/AVRG91_AVA_InitialStudyReport.pdf).
- [87] Arup, Redevelopment of So Uk Estate, Air Ventilation Assessment – Initial Study Report, Hong Kong Housing Authority, 2015. [https://www.pland.gov.hk/pland\\_en/info\\_serv/ava\\_register/ProjInfo/AVRG118\\_FinalReport.pdf](https://www.pland.gov.hk/pland_en/info_serv/ava_register/ProjInfo/AVRG118_FinalReport.pdf).
- [88] Arup, Planning and Design Study on the Redevelopment of Government Sites at Sai Yee Street and Mong Kok East Station – Feasibility Study, Hong Kong Planning Department, 2017. [https://www.pland.gov.hk/pland\\_en/info\\_serv/ava\\_register/ProjInfo/AVRG126\\_AVA\\_ISReport.pdf](https://www.pland.gov.hk/pland_en/info_serv/ava_register/ProjInfo/AVRG126_AVA_ISReport.pdf).
- [89] T. Uchida, T. Maruyama, Y. Ohya, New evaluation technique for WTG design wind speed using a CFD-model-based unsteady flow simulation with wind direction changes, *Model. Simul. Eng.* (2011).
- [90] A. Rasouli, H. Hangan, Microscale computational fluid dynamics simulation for wind mapping over complex topographic terrains, *ASME J. Sol. Energy Eng.* 135 (4) (2013), 041005.
- [91] CUHK, Urban Climatic Map and Standards for Wind Environment – Feasibility Study. Working Paper 1A, Draft Urban Climatic Analysis Map, 2008.
- [92] M. Schatzmann, H. Olesen, J. Franke, COST 732 Model Evaluation Case Studies: Approach and Results, University of Hamburg, Hamburg, Germany, 2010.
- [93] Australasian Wind Engineering Society, Wind Engineering Studies of Buildings, Australasian Wind Engineering Society, Queenstown, Australia, 2001.
- [94] American Society of Civil Engineers Task Committee on Manual of Practice for Wind Tunnel Testing of Buildings and Structures, Wind Tunnel Studies of Buildings and Structures, American Society of Civil Engineers, Reston, Virginia, 1999.
- [95] CLP Power Wind/Wave Tunnel Facility, Final Report for an Instructed Project at Ex-North Point Estate Site, – WWTF Investigation Report WWTF015-2008, The Hong Kong University of Science and Technology, 2008.
- [96] E. Willemsen, J.A. Wisse, Accuracy of assessment of wind speed in the built environment, *J. Wind Eng. Ind. Aerodyn.* 90 (2002) 1183–1190.
- [97] B. Blocken, T. Stathopoulos, J. Carmeliet, CFD simulation of the atmospheric boundary layer: wall function problems, *Atmos. Environ.* 41 (2007) 238–252.
- [98] B. Blocken, J. Carmeliet, T. Stathopoulos, CFD evaluation of wind speed conditions in passages between parallel buildings-effect of wall-function roughness modifications for the atmospheric boundary layer flow, *J. Wind Eng. Ind. Aerodyn.* 95 (2007) 941–962.
- [99] Z.T. Ai, C.M. Mak, CFD simulation of flow and dispersion around an isolated building: effect of inhomogeneous ABL and near-wall treatment, *Atmos. Environ.* 77 (2013) 568–578.
- [100] Y. Tominaga, T. Stathopoulos, Turbulent Schmidt numbers for CFD analysis with various types of flowfield, *Atmos. Environ.* 41 (2007) 8091–8099.
- [101] Y. Tominaga, T. Stathopoulos, CFD simulation of near-field pollutant dispersion in the urban environment: a review of current modeling techniques, *Atmos. Environ.* 79 (2013) 716–730.
- [102] B. Blocken, Computational Fluid Dynamics for urban physics: importance, scales, possibilities, limitations and ten tips and tricks towards accurate and reliable simulations, *Build. Environ.* 91 (2015) 219–245.
- [103] C. Garcia-Sanchez, G. Van Tendeloo, C. Gorle, Quantifying inflow uncertainties in RANS simulations of urban pollutant dispersion, *Atmos. Environ.* 161 (2017) 263–273.
- [104] A. Ricci, I. Kalkman, B. Blocken, M. Burlando, A. Freda, M.P. Repetto, Local-scale forcing effects on wind flows in an urban environment: impact of geometrical simplifications, *J. Wind Eng. Ind. Aerodyn.* 170 (2017) 238–255.
- [105] S. Liu, W. Pan, X. Zhao, H. Zhang, X. Cheng, Z. Long, Q. Chen, Influence of surrounding buildings on wind flow around a building predicted by CFD simulations, *Build. Environ.* 140 (2018) 1–10.